Finite volume method for self-consistent field theory of polymers: Material conservation and application

Daeseong Yong and Jaeup U. Kim*

Department of Physics, School of Natural Science, Ulsan National Institute of Science and Technology, Ulsan 44919, Republic of Korea

(Received 17 September 2017; revised manuscript received 7 November 2017; published 26 December 2017)

For the purpose of checking material conservation of various numerical algorithms used in the self-consistent-field theory (SCFT) of polymeric systems, we develop an algebraic method using matrix and bra-ket notation, which traces the Hermiticity of the product of the volume and evolution matrices. Algebraic tests for material conservation reveal that the popular pseudospectral method in the Cartesian grid conserves material perfectly, while the finite-volume method (FVM) is the proper tool when real-space SCFT with the Crank-Nicolson method is adopted in orthogonal coordinate systems. We also find that alternating direction implicit methods combined with the FVM exhibit small mass errors in the SCFT calculation. By introducing fractional cells in the FVM formulation, accurate SCFT calculations are performed for systems with irregular geometries and the results are consistent with previous experimental and theoretical works.

DOI: 10.1103/PhysRevE.96.063312

I. INTRODUCTION

The self-consistent-field theory (SCFT) is one of the most successful theories explaining statistical behavior of polymers and it has been especially powerful in predicting the nanostructures created by heterogeneous polymers [1–3]. In the SCFT, the statistics of polymers in the equilibrium state is described by partition functions of polymer chains residing in a self-consistently determined mean field. The partition functions are known to satisfy a partial differential equation in the form of a modified diffusion equation with the given initial conditions; thus, the typical way to obtain partition functions is to solve these partial differential equations.

In most practical polymer problems, the differential equation is impossible to solve analytically and one naturally adopts some numerical methods to find the solution. There are various numerical schemes developed to obtain the numerical solution of the modified diffusion equation. Among them, the pseudospectral method [4–10] and real-space method [10–20] are widely used for the accurate modeling of polymeric systems. The pseudospectral method, introduced by Rasmussen and Kalosakas [4] in this community, is proven to be highly efficient. It introduces operator splitting to separate the Laplacian part and the Laplacian is calculated in the Fourier space. After adopting numerical libraries for the Fourier and inverse Fourier transforms, the pseudospectral method is very intuitive and easy to implement.

For the real-space method, the finite-difference method (FDM) is the standard technique for solving the partial differential equations [16–18]. Its actual implementation may require additional effort, but it is at least intuitively structured and this method is unconditionally stable when the Crank-Nicolson method [21] is adopted. The Crank-Nicolson method, however, requires the solution of a banded matrix equation, which demands high computational costs. An attractive approximation of the Crank-Nicolson method is the alternating direction implicit (ADI) method, which only uses tridiagonal matrix equations and is also unconditionally stable. One additional advantage of the real-space method is that parallelization of the algorithm is very simple and efficient.

It has long been known that both the pseudospectral and real-space methods are plagued with the problem that they often fail to accurately conserve material, especially when curved coordinates are adopted. Like many other physical systems with real materials, violation of the conservation law in the process of numerical computation is one of the major concerns in the SCFT calculation. This problem is especially crucial for heterogeneous polymer systems with various possible phases. Because the field energy is proportional to the segment density, material error can cause a free energy error of similar order of magnitude. The free energy difference per chain between competing phases is usually small, so $10^{-3}k_BT$ of energy difference is often enough to disrupt the stability of a phase. This may be the order of the typical mass conservation error of a numerical scheme, depending on the parameter values and discretization methods; thus, for the accurate determination of the selected phase and phase boundaries, developing numerical methods with low material error is crucial [10,18]. Recently, Vorselaars *et al.* [19] introduced a hybrid of pseudospectral and real-space methods for a problem in the spherical coordinate system, and the finite-volume method (FVM) was adopted for the purpose of achieving better material conservation. However, only the r direction was discretized by the finite-volume approach in that work, and the utility of the FVM and its precise effect on the material conservation were not systematically tested.

Because of the presence of the potential fields and the fact that two partial partition functions work together to determine the segment density, the analysis of material conservation is quite complicated for the case of the SCFT. Conditions for the material conservation in the numerical implementation of the SCFT are not well established and the free energy convergence behavior is not fully understood, but there exist a few previous reports which analyze the mass error and free energy for the specific numerical methods they adopted [8,15,19,22].

In this paper we develop discretization methods of the modified diffusion equation using the FVM and we will pursue the mechanism of material conservation in the SCFT by an

*jukim@unist.ac.kr

algebraic analysis. Later, our numerical scheme will be used to solve a few interesting problems known to the polymer theory community. This paper is organized as follows. A standard SCFT is introduced in Sec. II and the formulation of our FVM follows in Sec. III. In Sec. IV we derive algebraic conditions for the material conservation of the numerical SCFT and a few popular numerical methods are tested using them. Our SCFT adopting the FVM is used to solve two problems with irregular geometries in Sec. V. We provide a brief discussion and summary in Sec. VI.

II. SELF-CONSISTENT-FIELD THEORY

In this section we make a brief introduction of the standard SCFT of infinitely flexible Gaussian chains. In this model the path of a chain labeled by i is represented by a curve $\mathbf{r}_i(s)$, where $s \in [0,1]$ is a continuous parameter following the backbone of the chain. For the given distribution of chains, the spatial segment density is obtained by $\hat{\phi}(\mathbf{r}) = (N/\rho_0)\sum_i \int_0^1 ds\, \delta(\mathbf{r} - \mathbf{r}_i(s))$, where N is the polymerization index and ρ_0^{-1} is the segment volume.

The SCFT is a mean field theory in which the original many-body problem is reduced to a one-body problem in a mean field; all the interactions between segments are represented by a mean potential field $w(\mathbf{r})$, which is determined by the ensemble average of the segment concentration $\phi(\mathbf{r}) \equiv \langle\hat{\phi}(\mathbf{r})\rangle$. As a prototypical case, the algebraic description of the SCFT for a system with identical n_p homopolymers is described below without a formal derivation.

The partial partition function for the first sN segments of a chain satisfies the modified diffusion equation

$$\frac{\partial}{\partial s}q(\mathbf{r},s) = \left[\frac{a^2N}{6}\nabla^2 - w(\mathbf{r})\right]q(\mathbf{r},s), \tag{1}$$

with the initial condition $q(\mathbf{r},0) = 1$. The complementary partial partition function for the last $(1-s)N$ segments is obtained by

$$-\frac{\partial}{\partial s}q^\dagger(\mathbf{r},s) = \left[\frac{a^2N}{6}\nabla^2 - w(\mathbf{r})\right]q^\dagger(\mathbf{r},s). \tag{2}$$

Note that the sign of the left-hand side is reversed because the function is evaluated from the $s = 1$ end with an initial condition $q^\dagger(\mathbf{r},1) = 1$.

The ensemble-average density of sNth segment at position $\mathbf{r}$, $\phi(\mathbf{r},s)$ must be proportional to the product of the two partial partition functions and the total density at position $\mathbf{r}$ is the sum of contributions from all segments. Thus,

$$\phi(\mathbf{r},s) = \frac{V_{\text{tot}}}{Q}q(\mathbf{r},s)q^\dagger(\mathbf{r},s), \tag{3}$$

$$\phi(\mathbf{r}) = \int_0^1 ds\, \phi(\mathbf{r},s), \tag{4}$$

where $V_{\text{tot}} = Nn_p/\rho_0$ is the total volume occupied by the polymer chains and the total partition function Q is defined as

$$Q[w] = \int d\mathbf{r}\, q(\mathbf{r},s)q^\dagger(\mathbf{r},s). \tag{5}$$

Note that even though Q is in principle independent of the choice of s for this integration, there exists a subtle issue regarding its dependence on s in its actual numerical calculation as we discuss later. The free energy of the homopolymer system for the given mean potential field $w(\mathbf{r})$ is

$$\frac{F}{n_p k_B T} = -\ln\frac{Q[w]}{V_{\text{tot}}} - \frac{1}{V_{\text{tot}}}\int d\mathbf{r}\, w(\mathbf{r})\phi(\mathbf{r}). \tag{6}$$

The self-consistency equations that the functions must satisfy depend on the physical situation one considers. For the case of the incompressible homopolymer melt, $w(\mathbf{r})$ must be iteratively updated until the output segment concentration satisfies the condition $\phi(\mathbf{r}) = 1$.

III. FINITE-VOLUME METHOD

The algebraic equations in the preceding section provide the exact mean field solution. However, only numerical solutions are available for most practical polymer problems and various errors are associated with the choice of the numerical scheme. One simple and typical choice is the FDM in which the space is discretized into grid points and all the differentiations are approximated by finite differences at the grid points. Unfortunately, the FDM often suffers in the precise conservation of the diffusing material when solving a diffusion problem in curved coordinates such as the cylindrical and spherical coordinate systems.

In solving the diffusion-type differential equations, one attractive alternative of the FDM is the FVM. Even though its final numerical formulation is very similar to that of the FDM, the FVM is conceptually different from the FDM in that it is based on the idea of flux conservation as explained below. For the rest of this section, we will explain our discretization scheme of the modified diffusion equation in the orthogonal coordinate systems using the FVM. Note that other types of FVMs are in principle available, but we claim that the method we introduce here is the best choice for the SCFT calculation in terms of simplicity and accuracy, as we explain in later sections.

The FVM is a method developed to solve partial differential equations while conserving important physical quantities using the idea of flux conservation. Integrating the differential equation in a small finite volume, the so-called grid cell, the integral can be converted to the difference of two functions by fundamental theorem of calculus in one dimension and the difference of two surface integrals using divergence theorem in higher dimensions. The resulting equation can be interpreted by using the concept of flux. Even though one makes an approximation for the function value on the cell surface, the FVM is always built to guarantee that the flux loss of one cell is equal to the gain in adjacent cells [23,24]. When solving a normal diffusion equation, this formulation guarantees the conservation of material, which is an important challenge in its numerical implementation.

For the description of our numerical scheme, we introduce a generic orthogonal coordinate system (x_1,x_2,x_3), with unit vectors $\hat{\mathbf{e}}_1$, $\hat{\mathbf{e}}_2$, and $\hat{\mathbf{e}}_3$. Its scale factors are given as (h_1,h_2,h_3). The vector $\mathbf{r} = (x_1,x_2,x_3)$ represents a position in this coordinate system and we will often use an integer- or half-integer-valued vector $\mathbf{i} = (i,j,k)$ to specify a discrete grid point; this position is often referred to as $\mathbf{r_i}$. The number of

grid points in each direction is I, J, and K, so the possible ranges of i, j, and k are $[\frac{1}{2}, I+\frac{1}{2}]$, $[\frac{1}{2}, J+\frac{1}{2}]$, and $[\frac{1}{2}, K+\frac{1}{2}]$, respectively, considering that the surface is $\frac{1}{2}$ grid away from the center of the cell. In order to describe an arbitrary direction, the index d is often used and sometimes the index is raised. For example, $\hat{\mathbf{e}}_d$ can represent any of $\hat{\mathbf{e}}_r$, $\hat{\mathbf{e}}_\theta$, and $\hat{\mathbf{e}}_\varphi$ for the spherical coordinate system. Also, $\mathbf{i} \pm \hat{\mathbf{e}}_d$ are used to represent an increment or decrement of the integer vector $\mathbf{i}$ in the $\hat{\mathbf{e}}_d$ direction by one step. For example, $\mathbf{i} \pm \hat{\mathbf{e}}_1$ imply new integer valued vectors $(i \pm 1, j, k)$ and $\mathbf{i} \pm \hat{\mathbf{e}}_2$ imply $(i, j \pm 1, k)$.

By defining $C_\mathbf{i}$ as the grid cell determined by the interval $x_1 \in [x_{1,i-1/2}, x_{1,i+1/2}]$, $x_2 \in [x_{2,j-1/2}, x_{2,j+1/2}]$, and $x_3 \in [x_{3,k-1/2}, x_{3,k+1/2}]$, its volume is given as

$$\Delta V_\mathbf{i} \equiv \int_{C_\mathbf{i}} dV = \int_{x_{3,k-1/2}}^{x_{3,k+1/2}} \int_{x_{2,j-1/2}}^{x_{2,j+1/2}} \int_{x_{1,i-1/2}}^{x_{1,i+1/2}} h_1 h_2 h_3 dx_1 dx_2 dx_3, \tag{7}$$

where $x_{d,i}$ represents the x_d position specified by the integer or half-integer i. For the case of equal grid spacing Δx_d, one can consider $x_{d,i} = x_{d,1} + (i-1)\Delta x_d$. With this volume segment definition, an integral is naturally converted to a discrete sum weighted by the cell volume

$$\int f(\mathbf{r}) d\mathbf{r} \to \sum_\mathbf{i} f_\mathbf{i} \Delta V_\mathbf{i}, \tag{8}$$

which will be our standard method of integration for the rest of this paper.

In the current finite-volume method, we sequentially evaluate the modified diffusion equation (1) after dividing the s direction into equal intervals Δs. Starting from the $s = 0$ end, after n evaluations, $q(\mathbf{r}, s_n)$ is obtained with $s_n = n\Delta s$. The purpose of the next FVM evaluation is to find $q(\mathbf{r}, s_{n+1})$ and it starts from integrating the original modified diffusion equation (1) by $\int_{C_\mathbf{i}} dV$ at the given $s = s_n$ value. The next step is to convert the volume integral of the Laplacian term to a surface integral using the divergence theorem. The result of the surface integral can be expressed as

$$\int_{A_\mathbf{i}} \nabla q(\mathbf{r}, s_n) \cdot d\mathbf{A} = \sum_{d=1,2,3} \left[F^d_{\mathbf{i}+(1/2)\hat{\mathbf{e}}_d} - F^d_{\mathbf{i}-(1/2)\hat{\mathbf{e}}_d} \right], \tag{9}$$

where $A_\mathbf{i}$ is the $\mathbf{i}$th cell surface and $F^d_{\mathbf{i}\pm(1/2)\hat{\mathbf{e}}_d}$ are the fluxes of $\nabla q(\mathbf{r}, s_n)$ crossing the two cell surfaces perpendicular to the unit vector $\hat{\mathbf{e}}_d$. The gradient of $q(\mathbf{r}, s_n)$,

$$\nabla q(\mathbf{r}, s_n) = \frac{1}{h_1} \frac{\partial q(\mathbf{r}, s_n)}{\partial x_1} \hat{\mathbf{e}}_1 + \frac{1}{h_2} \frac{\partial q(\mathbf{r}, s_n)}{\partial x_2} \hat{\mathbf{e}}_2 + \frac{1}{h_3} \frac{\partial q(\mathbf{r}, s_n)}{\partial x_3} \hat{\mathbf{e}}_3, \tag{10}$$

can be approximated by using the difference of $q^n_\mathbf{i} \equiv \langle q(\mathbf{r}, s_n) \rangle_\mathbf{i}$ between adjacent cells, where $\langle\,\rangle_\mathbf{i}$ implies the volume average within the cell $C_\mathbf{i}$. Applying this, the fluxes are now approximated as

$$F^d_{\mathbf{i}\pm(1/2)\hat{\mathbf{e}}_d} \cong \pm \Delta A^d_{\mathbf{i}\pm(1/2)\hat{\mathbf{e}}_d} \frac{q^n_{\mathbf{i}\pm\hat{\mathbf{e}}_d} - q^n_\mathbf{i}}{h^{d\pm}_\mathbf{i} \Delta x_d}, \tag{11}$$

where $\Delta A^d_{\mathbf{i}\pm(1/2)\hat{\mathbf{e}}_d}$ are the areas of the two cell surfaces perpendicular to the vector $\hat{\mathbf{e}}_d$ and $h^{d\pm}_\mathbf{i}$ are the values of the scale factor h_d at the midpoint of each surface. Using this expression, the discrete Laplacian operator in each direction becomes

$$\delta^2_d q^n_\mathbf{i} = B^{d+}_\mathbf{i} \left(q^n_{\mathbf{i}+\hat{\mathbf{e}}_d} - q^n_\mathbf{i} \right) - B^{d-}_\mathbf{i} \left(q^n_\mathbf{i} - q^n_{\mathbf{i}-\hat{\mathbf{e}}_d} \right), \tag{12a}$$

$$B^{d\pm}_\mathbf{i} \equiv \frac{\Delta A^d_{\mathbf{i}\pm(1/2)\hat{\mathbf{e}}_d}}{h^{d\pm}_\mathbf{i} \Delta x_d \Delta V_\mathbf{i}}. \tag{12b}$$

The top surface of the cell $C_\mathbf{i}$ defined by $\Delta A^d_{\mathbf{i}+(1/2)\hat{\mathbf{e}}_d}$ is equal to the bottom surface of the cell $C_{\mathbf{i}+\hat{\mathbf{e}}_d}$ expressed as $\Delta A^d_{(\mathbf{i}+\hat{\mathbf{e}}_d)-(1/2)\hat{\mathbf{e}}_d}$ and the midpoint of the top surface of the cell $C_\mathbf{i}$ is also equal to that of the bottom surface of the cell $C_{\mathbf{i}+\hat{\mathbf{e}}_d}$. This implies that $h^{d+}_\mathbf{i} = h^{d-}_{\mathbf{i}+\hat{\mathbf{e}}_\mathbf{d}}$ and the following equation can be confirmed:

$$B^{d+}_\mathbf{i} \Delta V_\mathbf{i} = B^{d-}_{\mathbf{i}+\hat{\mathbf{e}}_d} \Delta V_{\mathbf{i}+\hat{\mathbf{e}}_d}. \tag{13}$$

This is one of the most important characteristics of the FVM we implement here and it provides an essential tool in the material conservation analysis in later sections. Note that this equation is only occasionally satisfied for the FDM. When the standard three-point FDM is used, Eq. (13) is satisfied in the Cartesian coordinate system, but it is not valid in the cylindrical and spherical coordinate systems.

As mentioned earlier in this section, this generic FVM can in principle be applied to any orthogonal coordinate systems. From now on, we take the spherical coordinate system as an example, because it is the least nontrivial case among the three popular coordinate systems. Note that we show a two-dimensional version of the FVM for simplicity and its three-dimensional generalization is a trivial task because the grids are equally spaced in the φ direction and the cell volumes do not vary in that direction. For those who are interested in the detailed derivation, see Appendix A, which presents the three-dimensional FVM formulation for the cylindrical coordinate system.

In the spherical coordinate system, the variables are $(x_1, x_2, x_3) = (r, \theta, \varphi)$ and the scale factors are $(h_1, h_2, h_3) = (1, r, r\sin\theta)$. Two-dimensional spherical grids and cells are illustrated in Fig. 1. The areas of the two surfaces of the cell $C_{i,j}$ perpendicular to $\hat{\mathbf{e}}_r$ are $\Delta A^r_{i\pm1/2,j} = \int_0^{2\pi} \int_{\theta_{j-1/2}}^{\theta_{j+1/2}} r^2_{i\pm1/2} \sin\theta \, d\theta \, d\varphi$. The areas of the cell surfaces perpendicular to $\hat{\mathbf{e}}_\theta$ are the differences of lateral surface areas of two cones $\Delta A^\theta_{i,j\pm1/2} = \int_0^{2\pi} \int_{r_{i-1/2}}^{r_{i+1/2}} r \sin\theta_{j\pm1/2} dr \, d\varphi$ and the volume of the cell $C_{i,j}$ is given as $\Delta V_{i,j} = \int_0^{2\pi} \int_{\theta_{j-1/2}}^{\theta_{j+1/2}} \int_{r_{i-1/2}}^{r_{i+1/2}} r^2 \sin\theta \, dr \, d\theta \, d\varphi$. All these calculations can be done analytically, and by combining these results, one can obtain the geometric factors for the flux calculation $B^{d\pm}_\mathbf{i}$, as defined in Eq. (12b). Using the scale factors for the two-dimensional spherical coordinate system, $h^{r\pm}_{i,j} = 1$ and $h^{\theta\pm}_{i,j} = r_i$, the results are

$$B^{r\pm}_{i,j} = \frac{\Delta A^r_{i\pm1/2,j}}{\Delta r \Delta V_{i,j}} = \frac{r^2_{i\pm1/2}}{\Delta r \left(r^3_{i+1/2} - r^3_{i-1/2} \right)}, \tag{14a}$$

$$B^{\theta\pm}_{i,j} = \frac{\Delta A^\theta_{i,j\pm1/2}}{r_i \Delta\theta \Delta V_{i,j}} = \frac{\sin\theta_{j\pm1/2}}{\Delta\theta \left(r_i^2 + \Delta r^2/12 \right) (\cos\theta_{j-1/2} - \cos\theta_{j+1/2})}. \tag{14b}$$

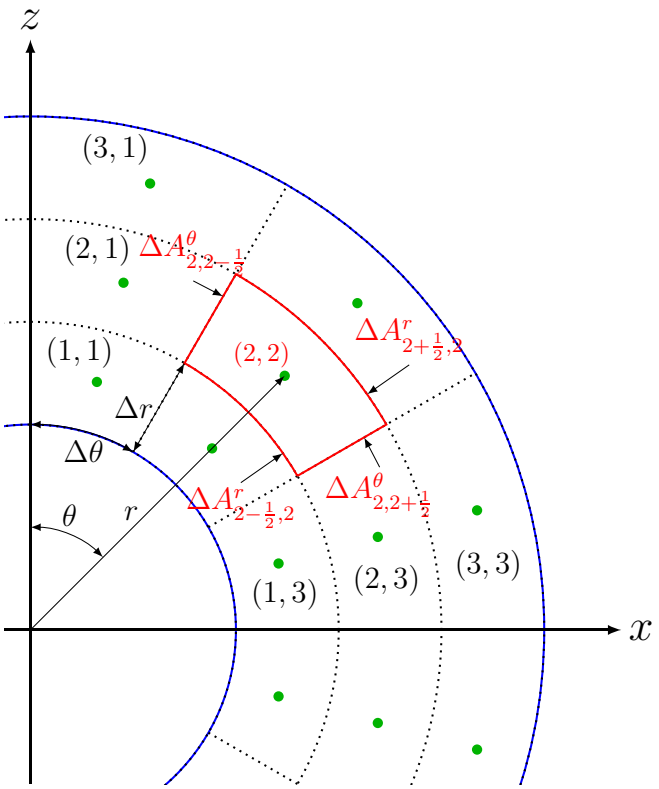

FIG. 1. Pictorial representation of the discretized spherical coordinate system in two dimensions for the case of $I = 3$, $J = 6$, $r_1 = 5\Delta r/2$, $\theta_1 = \Delta\theta/2$, and $\Delta\theta = \pi/6$. The system boundary is at $r_{1/2} = 2\Delta r$ and $r_{3+1/2} = 5\Delta r$ in the r direction and at $\theta_{1/2} = 0$ and $\theta_{6+1/2} = \pi$ in the θ direction. Each green dot represents a grid point $\mathbf{i} = (i, j)$ and the neighboring region surrounded by dotted lines indicates the grid cell $C_\mathbf{i}$. The cell $C_{2,2}$ is highlighted with red lines as an example.

Using this FVM formulation, we are now ready to convert the modified diffusion equation (1) to successive discretized operations. Applying the standard Crank-Nicolson method, the evolution equation of $q_\mathbf{i}^n$ is obtained as

$$\left(1 - a^2 N \frac{\Delta s}{12}\delta^2 + \frac{\Delta s}{2} w_\mathbf{i}\right) q_\mathbf{i}^{n+1} \cong \left(1 + a^2 N \frac{\Delta s}{12}\delta^2 - \frac{\Delta s}{2} w_\mathbf{i}\right) q_\mathbf{i}^n, \tag{15}$$

where the field term is defined by $w_\mathbf{i} = \langle w(\mathbf{r})\rangle_\mathbf{i}$. The discretized conjugate partial partition function $q_\mathbf{i}^{\dagger n}$, which is defined as $\langle q^\dagger(\mathbf{r}, s_{N-n})\rangle_\mathbf{i}$, follows the same evolution equation. Note that the FDM can be expressed in exactly the same way, except that the geometric factor (12b) and the discretized Laplacian operator (12a) differ slightly from the FVM version. The truncation error of the above FVM is calculated to be $O(\Delta s^3) + \sum_d O(\Delta s \Delta x_d^2)$ for both the cylindrical and spherical coordinate systems.

IV. MATERIAL CONSERVATION

If we assume that all the q's are obtained by successively evaluating Eq. (15) using either the FDM or FVM, one can check the material conservation of each numerical scheme in the following way. Summing both sides of Eq. (15) over all cells,

$$\begin{aligned}\sum_\mathbf{i} \Delta V_\mathbf{i} \Bigg[&\left(1 + \frac{\Delta s}{2} w_\mathbf{i}\right) q_\mathbf{i}^{n+1} - a^2 N \frac{\Delta s}{12} \sum_d B_\mathbf{i}^{d+} \left(q_{\mathbf{i}+\hat{\mathbf{e}}_d}^{n+1} - q_\mathbf{i}^{n+1}\right) \\ &- B_\mathbf{i}^{d-} \left(q_\mathbf{i}^{n+1} - q_{\mathbf{i}-\hat{\mathbf{e}}_d}^{n+1}\right) \Bigg] \\ = \sum_\mathbf{i} \Delta V_\mathbf{i} \Bigg[&\left(1 - \frac{\Delta s}{2} w_\mathbf{i}\right) q_\mathbf{i}^{n} + a^2 N \frac{\Delta s}{12} \sum_d B_\mathbf{i}^{d+} \left(q_{\mathbf{i}+\hat{\mathbf{e}}_d}^{n} - q_\mathbf{i}^{n}\right) \\ &- B_\mathbf{i}^{d-} \left(q_\mathbf{i}^{n} - q_{\mathbf{i}-\hat{\mathbf{e}}_d}^{n}\right) \Bigg].\end{aligned} \tag{16}$$

When the field term $w_\mathbf{i}$ vanishes and the FVM is adopted, using Eq. (13), it is straightforward to show that the discrete sum of the partial partition function weighted by the cell volume is invariant,

$$\sum_\mathbf{i} q_\mathbf{i}^n \Delta V_\mathbf{i} = \sum_\mathbf{i} q_\mathbf{i}^{n+1} \Delta V_\mathbf{i}. \tag{17}$$

For typical diffusion problems, the function at the position of our $q_\mathbf{i}^n$ is the material density at the nth time step. The above analysis shows that the FVM conserves the amount of diffusing material for those problems provided there exists no field term. In the FVM, even though the flux at the cell surface is approximated, it is guaranteed that one cell's flux loss becomes another cell's flux gain and this is the fundamental reason why it is generally regarded that the numerical schemes using the FVM conserve material.

For the case of the SCFT adopting the modified diffusion equation, however, Eq. (17) is not guaranteed because of the field term. It is obvious that the introduction of the field term creates or annihilates materials for the normal diffusion equation and it is meaningless to discuss the material conservation. However, this does not necessarily mean that material conservation must be violated in the numerical solution of the SCFT. In the SCFT, the discrete volume integral of the segment concentration, rather than that of the partial partition function, is required to be invariant for the material conservation. This material conservation property has never been investigated in a systematic way. In this section, the general condition for the material conservation will be derived and its validity will be tested for a few widely used numerical methods of the SCFT.

For an efficient analysis of the material conservation, we express the state of the discretized partial partition function as a column vector and the evolution of the partial partition function is expressed as a matrix operator acting on the column vector. For further simplification, this matrix algebra will be expressed in the standard bra-ket notation commonly used in quantum mechanics. Its validity and efficiency will be apparent as discussion continues. Note that we demonstrate the two-dimensional version of the analysis, but its three-dimensional generalization is straightforward and the conclusions in the following sections are essentially identical in higher dimensions.

A. Conditions for material conservation

In this section we will derive the basic condition for a given numerical scheme to conserve material in the SCFT using the bra-ket algebra. In the matrix and bra-ket notation, the two partial partition functions are expressed as

$$|q^n\rangle = \left(q^n_{1,1}\ q^n_{1,2}\ \cdots\ q^n_{1,J}\ q^n_{2,1}\ \cdots\ q^n_{I,J}\right)^T, \tag{18a}$$

$$|p^n\rangle = \left(q^{\dagger n}_{1,1}\ q^{\dagger n}_{1,2}\ \cdots\ q^{\dagger n}_{1,J}\ q^{\dagger n}_{2,1}\ \cdots\ q^{\dagger n}_{I,J}\right)^T. \tag{18b}$$

Note that the original two-dimensional discrete functions are now packed into one-dimensional column vectors and we use p^n instead of $q^{\dagger n}$ for the purpose of avoiding confusion in the bra-ket notation. The evolution operator acting on $|q^n\rangle$ to produce $|q^{n+1}\rangle$ can be defined in the form

$$|q^{n+1}\rangle = \mathcal{U}|q^n\rangle, \quad |p^{n+1}\rangle = \mathcal{U}|p^n\rangle, \tag{19}$$

where all the matrix elements of $|q^n\rangle$ and $|p^n\rangle$ are real. For the purpose of distinction, matrices or operators will be represented by calligraphic characters from now on. The actual shape of $\mathcal{U}$ depends on the numerical scheme we choose. Also, for the case of AB diblock copolymers, the shape of $\mathcal{U}$ switches at the AB block junction point, but the material conservation analysis is the same as the homopolymer case we describe below.

In this matrix representation, the cell volume ΔV_{ij} is expressed as the diagonal matrix

$$\mathcal{V} = \begin{pmatrix} \Delta V_{1,1} & & & & & & \\ & \Delta V_{1,2} & & & 0 & & \\ & & \ddots & & & & \\ & & & \Delta V_{i,j} & & & \\ & & & & \ddots & & \\ & 0 & & & & \Delta V_{I,J-1} & \\ & & & & & & \Delta V_{I,J} \end{pmatrix}. \tag{20}$$

Writing the segment concentration equation (3) in the discrete version, the smth segment concentration can be calculated after m evolutions of $q^0_{\mathbf{i}}$ and $N-m$ evolutions of $q^{\dagger 0}_{\mathbf{i}}$. The concentration at cell $C_{\mathbf{i}}$ can be written as

$$\phi_{\mathbf{i},m} = \frac{V_{\text{tot}}}{N Q_n} q^m_{\mathbf{i}} q^{\dagger(N-m)}_{\mathbf{i}}. \tag{21}$$

Taking the advantage of the bra-ket notation, Eq. (5) is now expressed in the simple algebraic form

$$\begin{aligned} Q_n &= \sum_{\mathbf{i}} q^n_{\mathbf{i}} q^{\dagger(N-n)}_{\mathbf{i}} \Delta V_{\mathbf{i}} = \langle q^n|\mathcal{V}|p^{N-n}\rangle \\ &= \langle q^0|(\mathcal{U}^\dagger)^n \mathcal{V}\mathcal{U}^{N-n}|p^0\rangle. \end{aligned} \tag{22}$$

In the above equations, we keep the subscript n for Q, which is the total partition function evaluated at $s = s_n$. In the formal introduction of the SCFT, we emphasized that Q must be independent of s. However, because we are making an approximated numerical calculation, it is not guaranteed that Q_n is independent of n.

As a measure to track the material conservation, let us define the dimensionless global volume error as

$$\begin{aligned} \epsilon_{V,m} &\equiv \frac{N}{V_{\text{tot}}}\left(\sum_{\mathbf{i}} \phi_{\mathbf{i},m+1}\Delta V_{\mathbf{i}} - \sum_{\mathbf{i}} \phi_{\mathbf{i},m}\Delta V_{\mathbf{i}}\right) \\ &= \frac{1}{Q_n}\langle q^m|(\mathcal{U}^\dagger\mathcal{V} - \mathcal{V}\mathcal{U})|p^{N-m-1}\rangle, \end{aligned} \tag{23}$$

where the latter equation can be obtained using Eq. (21). We seek the condition that this mass error always becomes zero, regardless of the choice of the following parameters: (i) real field $w(\mathbf{r})$, (ii) contour step size Δs, (iii) contour step number N, and (iv) initial conditions of partition functions $q(\mathbf{r},0)$ and $q^\dagger(\mathbf{r},1)$. The sufficient and necessary condition for the material conservation to be valid at all situations is that the evolution matrix satisfies the equation

$$(\mathcal{V}\mathcal{U})^\dagger = \mathcal{V}\mathcal{U}, \tag{24}$$

i.e., $\mathcal{V}\mathcal{U}$ must be a Hermitian operator or matrix, and this is all we need to test each numerical method. In addition, this condition also guarantees that Q_n in Eq. (22) is independent of n. For the rest of this section we will investigate the validity of Eq. (24) for various numerical methods commonly used in the evaluation of the SCFT equations.

B. Pseudospectral method

Nowadays, in the polymer theory community, the pseudospectral method is commonly used for the solution of the SCFT in Cartesian coordinates [4,5,10,25]. Even though our major focus has been on the real-space method using the FDM or FVM, it is perfectly fine to apply Eq. (24) to check the material conservation of the pseudospectral method. Let us begin our discussion with the standard pseudospectral method in the two-dimensional Cartesian coordinate system (x,y) with periodic boundary conditions in both directions. For the start of the pseudospectral method, Strang splitting is applied to the modified diffusion equation

$$\begin{aligned} q(\mathbf{r},s+\Delta s) \cong\ & \exp\left(-\frac{\Delta s w(\mathbf{r})}{2}\right)\exp\left(\frac{a^2 N \Delta s \nabla^2}{6}\right) \\ & \times \exp\left(-\frac{\Delta s w(\mathbf{r})}{2}\right) q(\mathbf{r},s). \end{aligned} \tag{25}$$

The first step is to calculate $\exp[-\Delta s w(\mathbf{r})/2]q(\mathbf{r},s)$ in the real space. Using the bra-ket notation in the discrete world, it can be written as $\mathcal{X}|q^n\rangle$, where $\mathcal{X} \equiv \exp(-\mathcal{W})$ and $\mathcal{W}$ is the following diagonal matrix representing the effect of field:

$$\mathcal{W} = \frac{\Delta s}{2}\begin{pmatrix} w_{1,1} & & & & \\ & w_{1,2} & & 0 & \\ & & \cdots & & \\ & 0 & & w_{I,J-1} & \\ & & & & w_{I,J} \end{pmatrix}. \tag{26}$$

The next step is to perform the two-dimensional discrete Fourier transform (DFT). One possible choice of the DFT

operator $\mathcal{F}$ is

$$\begin{pmatrix} 1 & 1 & 1 & \cdots & 1 & 1 & 1 & \cdots \\ 1 & \lambda & \lambda^2 & \cdots & \lambda^{J-1} & 1 & \lambda & \cdots \\ 1 & \lambda^2 & \lambda^4 & \cdots & \lambda^{2(J-1)} & 1 & \lambda^2 & \cdots \\ & & & \ddots & & & & \ddots \\ 1 & \lambda^{J-1} & \lambda^{2(J-1)} & \cdots & \lambda^{(J-1)(J-1)} & 1 & \lambda^{J-1} & \cdots \\ 1 & 1 & 1 & \cdots & 1 & \omega & \omega & \cdots \\ 1 & \lambda & \lambda^2 & \cdots & \lambda^{J-1} & \omega & \omega\lambda & \cdots \\ & & & \ddots & & & & \ddots \end{pmatrix} \tag{27}$$

divided by $\sqrt{IJ}$, where $\omega = \exp(2\pi i/I)$ and $\lambda = \exp(2\pi i/J)$ are the principal Ith and Jth roots of unity, respectively. With this choice of DFT, the inverse DFT operator is simply the inverse of the $\mathcal{F}$ matrix, $\mathcal{F}^{-1}$, and it is easy to confirm $\mathcal{F}^{-1} = \mathcal{F}^{\dagger}$. The next task is to apply the $\exp(a^2 N \Delta s \nabla^2/6)$ operator in the Fourier space, which is a multiplication of a real diagonal matrix with the shape

$$\mathcal{C} = \begin{pmatrix} c_{1,1} & & & & & \\ & c_{1,2} & & & 0 & \\ & & c_{1,3} & & & \\ & & & \ddots & & \\ & 0 & & & c_{I,J-1} & \\ & & & & & c_{I,J} \end{pmatrix}. \tag{28}$$

The last step is to perform an inverse DFT and to multiply $\mathcal{X}$, and the final evolution matrix becomes $\mathcal{U} = \mathcal{X}\mathcal{F}^{-1}\mathcal{C}\mathcal{F}\mathcal{X}$. The boundaries are periodic and thus it is natural to take all the cell volumes to be uniform $\mathcal{V} = \Delta x \Delta y \mathcal{I}$, where $\mathcal{I}$ is an identity matrix. This means that the $\mathcal{U}$ operator or the matrix $\mathcal{X}\mathcal{F}^{-1}\mathcal{C}\mathcal{F}\mathcal{X}$ only needs to be Hermitian for the material conservation. Since $(\mathcal{X}\mathcal{F}^{-1}\mathcal{C}\mathcal{F}\mathcal{X})^{\dagger} = \mathcal{X}\mathcal{F}^{\dagger}\mathcal{C}(\mathcal{F}^{-1})^{\dagger}\mathcal{X} = \mathcal{X}\mathcal{F}^{-1}\mathcal{C}\mathcal{F}\mathcal{X}$, the matrix $\mathcal{V}\mathcal{U}$ is Hermitian and the material conservation is confirmed. It is possible to apply this proof to the higher-order pseudospectral method proposed by Ranjan *et al.* [7,8] and the three-dimensional generalization of this proof is also straightforward.

For other boundary conditions, discrete sine and cosine transforms are often used in the pseudospectral method and half-size cells may be used at the boundaries. Even though the above proof is not directly applicable to those cases, such a problem is mathematically equivalent to a periodic boundary problem with twice the size of the original system and the above proof guarantees the material conservation of those systems.

C. Crank-Nicolson method

In this section we check the material conservation for the Crank-Nicolson method. Note that there are a few choices for the implementation of the Crank-Nicolson method. Both the FDM and FVM can be combined with it and field operator splitting consistent with Eq. (25) may or may not be used. All these choices will be discussed here.

As explained at the end of Sec. III, when the Crank-Nicolson method without operator splitting is adopted, the partial partition function evolves according to the algebraic equation

$$\left(1 - a^2 N \frac{\Delta s}{12}\delta^2 + \frac{\Delta s}{2} w_{\mathbf{i}}\right) q_{\mathbf{i}}^{n+1} = \left(1 + a^2 N \frac{\Delta s}{12}\delta^2 - \frac{\Delta s}{2} w_{\mathbf{i}}\right) q_{\mathbf{i}}^{n}. \tag{29}$$

For the two-dimensional case, the discrete Laplacian operator has two directional components $\delta^2 \equiv \delta_1^2 + \delta_2^2$ and each of them can be expressed by $\delta_d^2 q_{\mathbf{i}}^n = B_{\mathbf{i}}^{d+}(q_{\mathbf{i}+\hat{\mathbf{e}}_d}^n - q_{\mathbf{i}}^n) - B_{\mathbf{i}}^{d-}(q_{\mathbf{i}}^n - q_{\mathbf{i}-\hat{\mathbf{e}}_d}^n)$ using the three-point FDM or FVM. Writing Eq. (29) in the bra-ket form,

$$(\mathcal{I} - \mathcal{O} + \mathcal{W})|q^{n+1}\rangle = (\mathcal{I} + \mathcal{O} - \mathcal{W})|q^{n}\rangle, \tag{30}$$

where the rescaled discrete Laplacian operator $\mathcal{O}$ has a nearly banded shape when written in a matrix form. All the nonzero components of $\mathcal{O}$ are either $O_{\mathbf{i}}^{d\pm} \equiv aN^2 \Delta s B_{\mathbf{i}}^{d\pm}/12$ or their linear combinations. One example of $\mathcal{O}$ is shown in Fig. 2. The following discussion is based on the matrix shape of $\mathcal{O}$ for the periodic boundary conditions. It is easy to confirm that the conclusion is the same for the Dirichlet and Neumann boundary conditions, because the resultant $\mathcal{O}$ matrix essentially has the same structure.

Using operator algebra, let us now derive conditions that the components of $\mathcal{O}$ must satisfy for the material conservation. To begin with, we assume that $\mathcal{I} - \mathcal{O} + \mathcal{W}$ is invertible, otherwise $|q^{n+1}\rangle$ cannot be determined by Eq. (30). By multiplying $(\mathcal{I} - \mathcal{O} + \mathcal{W})^{-1}$ on both sides of Eq. (30), one gets

$$|q^{n+1}\rangle = (\mathcal{I} - \mathcal{O} + \mathcal{W})^{-1}(\mathcal{I} + \mathcal{O} - \mathcal{W})|q^{n}\rangle \equiv \mathcal{U}|q^{n}\rangle. \tag{31}$$

As explained earlier, $\mathcal{V}\mathcal{U} = \mathcal{V}(\mathcal{I} - \mathcal{O} + \mathcal{W})^{-1}(\mathcal{I} + \mathcal{O} - \mathcal{W})$ must be Hermitian for the material conservation. This expression is simplified as

$$\begin{aligned} &\mathcal{V}(\mathcal{I} - \mathcal{O} + \mathcal{W})^{-1}(\mathcal{I} + \mathcal{O} - \mathcal{W}) \\ &\quad = \mathcal{V}(\mathcal{I} - \mathcal{O} + \mathcal{W})^{-1}[2\mathcal{I} - (\mathcal{I} - \mathcal{O} + \mathcal{W})] \\ &\quad = 2\mathcal{V}(\mathcal{I} - \mathcal{O} + \mathcal{W})^{-1} - \mathcal{V}. \end{aligned} \tag{32}$$

Since the multiplication of a constant and the addition of a real diagonal matrix do not affect the Hermiticity property of a matrix, we only need to check if the following matrix is Hermitian:

$$\mathcal{V}(\mathcal{I} - \mathcal{O} + \mathcal{W})^{-1}. \tag{33}$$

Using the fact that a matrix and its inverse are both Hermitian or non-Hermitian at the same time, it is enough to check the Hermiticity of the expression

$$(\mathcal{I} - \mathcal{O} + \mathcal{W})\mathcal{V}^{-1}. \tag{34}$$

Because $(\mathcal{I} + \mathcal{W})\mathcal{V}^{-1}$ is diagonal, the Hermiticity relation we need to test is the equation

$$\mathcal{O}\mathcal{V}^{-1} = \mathcal{V}^{-1}\mathcal{O}^{\dagger}. \tag{35}$$

After multiplying $\mathcal{V}$ once from the left and once from the right, the final Hermiticity relation becomes

$$\mathcal{V}\mathcal{O} = (\mathcal{V}\mathcal{O})^{\dagger}. \tag{36}$$

One cannot get any further with the operator algebra, but because we know the generic shape of the $\mathcal{O}$ matrix, we

$$\begin{pmatrix}
 & & & & O^{r+}_{1,1} & 0 & 0 & 0 & \\
 & & & & 0 & O^{r+}_{1,2} & 0 & 0 & \\
 & & \cdots & & 0 & 0 & O^{r+}_{1,3} & 0 & \\
 & & & & 0 & 0 & 0 & O^{r+}_{1,4} & \\
O^{r-}_{2,1} & 0 & 0 & 0 & -O^{r-}_{2,1}-O^{r+}_{2,1}-O^{\theta-}_{2,1}-O^{\theta+}_{2,1} & O^{\theta+}_{2,1} & 0 & O^{\theta-}_{2,1} & \cdots \\
0 & O^{r-}_{2,2} & 0 & 0 & O^{\theta-}_{2,2} & -O^{r-}_{2,2}-O^{r+}_{2,2}-O^{\theta-}_{2,2}-O^{\theta+}_{2,2} & O^{\theta+}_{2,2} & 0 & \\
0 & 0 & O^{r-}_{2,3} & 0 & 0 & O^{\theta-}_{2,3} & -O^{r-}_{2,3}-O^{r+}_{2,3}-O^{\theta-}_{2,3}-O^{\theta+}_{2,3} & O^{\theta+}_{2,3} & \\
0 & 0 & 0 & O^{r-}_{2,4} & O^{\theta+}_{2,4} & 0 & O^{\theta-}_{2,4} & -O^{r-}_{2,4}-O^{r+}_{2,4}-O^{\theta-}_{2,4}-O^{\theta+}_{2,4} & \\
 & & & & & \vdots & & & \ddots
\end{pmatrix}$$

FIG. 2. The $\mathcal{O}$ matrix for a 12-point (3×4) discretized domain in the two-dimensional spherical coordinate system, with $i \in [1,3]$ and $j \in [1,4]$. Only part of the 12×12 matrix is shown. If Neumann boundary conditions are chosen in the r direction, $O^{r-}_{1,j}$ and $O^{r+}_{3,j}$ become zeros.

can directly compare the shape of $(\mathcal{V}\mathcal{O})^\dagger$ and $\mathcal{V}\mathcal{O}$ to find the equivalent expression

$$O^{d+}_{\mathbf{i}} \Delta V_{\mathbf{i}} = O^{d-}_{\mathbf{i}+\hat{\mathbf{e}}_d} \Delta V_{\mathbf{i}+\hat{\mathbf{e}}_d}, \tag{37}$$

which is essentially the same as Eq. (13) considering $O^{d\pm}_{\mathbf{i}} = aN^2 \Delta s B^{d\pm}_{\mathbf{i}}/12$. This completes the proof that the FVM we formulated in Sec. III always conserves the amount of material when the two-dimensional (2D) Crank-Nicolson method without operator splitting is adopted to solve the SCFT equations.

Let us now consider the following shape of the evolution equation, which we call the 2D Crank-Nicolson method with operator splitting [22]:

$$\left(1 - a^2 N \frac{\Delta s}{12}\delta^2\right) \exp\left(\frac{\Delta s}{2} w_{\mathbf{i}}\right) q^{n+1}_{\mathbf{i}} = \left(1 + a^2 N \frac{\Delta s}{12}\delta^2\right) \exp\left(-\frac{\Delta s}{2} w_{\mathbf{i}}\right) q^{n}_{\mathbf{i}}. \tag{38}$$

In this case, the evolution matrix $\mathcal{U}$ is $\mathcal{X}(\mathcal{I}-\mathcal{O})^{-1}(\mathcal{I}+\mathcal{O})\mathcal{X}$, assuming that $\mathcal{I}-\mathcal{O}$ is invertible. The two $\mathcal{X}$ matrices in this equation are removable in checking the Hermiticity of the matrix (see Appendix B) and thus we only need to check the Hermiticity of the expression $\mathcal{V}(\mathcal{I}-\mathcal{O})^{-1}(\mathcal{I}+\mathcal{O})$, which is just the same as the previous case with $\mathcal{W}=0$. All the arguments we used from Eqs. (31)–(37) are valid when $\mathcal{W}=0$ and thus our FVM formulation conserves the amount of material when the 2D Crank-Nicolson method with operator splitting is adopted to solve the SCFT equations.

It is the proper time to discuss the material conservation of the 2D Crank-Nicolson method with the combination of the FDM. In general, the geometric factors $B^{d\pm}_{\mathbf{i}}$ of the FDM are different from those of the FVM. Taking the three-point FDM in the spherical coordinate system as an example, the discrete Laplacian operator in each direction becomes $B^{r\pm}_{i,j} = \frac{1}{\Delta r^2}(1 \pm \frac{\Delta r}{r_i})$ and $B^{\theta\pm}_{i,j} = \frac{1}{r_i^2 \Delta\theta^2}(1 \pm \frac{\Delta\theta}{2\tan\theta_j})$. By checking Eq. (37) for a few points, it is easy to confirm that material conservation is violated when FDM geometric factors are adopted. The only exception is the Cartesian coordinate system for which the FDM can be made to be equivalent to the FVM by simply setting $B^{x\pm}_{i,j} = 1/\Delta x^2$ and $B^{y\pm}_{i,j} = 1/\Delta y^2$. In conclusion, the FVM with the 2D Crank-Nicolson method conserves the amount of material in the SCFT regardless of the use of the operator splitting method. The FDM has this property only for the Cartesian coordinate system.

D. Alternating direction implicit method

Even though the Crank-Nicolson method is almost always a preferable choice in terms of accuracy, it inevitably introduces a complicated implicit matrix equation and further approximation is often recommended for fast calculation of the partial partition functions. One attractive strategy is to split the matrix equation into many matrix equations, each of which treats only one direction implicitly; this approach is collectively called the ADI method [10,18,21,22,26–31]. Among them, the following basic ADI method is most famous, and this will be our starting point for the discussion of the material conservation of ADI methods.

The basic ADI method for the two-dimensional system without operator splitting is given as the two-step algebraic equations

$$\left(1 - a^2 N \frac{\Delta s}{12}\delta_2^2\right) q^{n+1/2}_{\mathbf{i}} = \left(1 + a^2 N \frac{\Delta s}{12}\delta_1^2 - \frac{\Delta s}{2} w_{\mathbf{i}}\right) q^{n}_{\mathbf{i}}, \tag{39a}$$

$$\left(1 - a^2 N \frac{\Delta s}{12}\delta_1^2 + \frac{\Delta s}{2} w_{\mathbf{i}}\right) q^{n+1}_{\mathbf{i}} = \left(1 + a^2 N \frac{\Delta s}{12}\delta_2^2\right) q^{n+1/2}_{\mathbf{i}}. \tag{39b}$$

It can be written in the bra-ket form

$$(\mathcal{I}-\mathcal{O}_2)|q^{n+1/2}\rangle = (\mathcal{I}+\mathcal{O}_1-\mathcal{W})|q^n\rangle, \tag{40a}$$

$$(\mathcal{I}-\mathcal{O}_1+\mathcal{W})|q^{n+1}\rangle = (\mathcal{I}+\mathcal{O}_2)|q^{n+1/2}\rangle, \tag{40b}$$

where $\mathcal{O}_1$ and $\mathcal{O}_2$ are x_1 and x_2 directional operator matrices (see Figs. 3 and 4), respectively, and they satisfy $\mathcal{O}_1+\mathcal{O}_2=\mathcal{O}$. In order to verify the material conservation, it is required to check if the following matrix is Hermitian:

$$\mathcal{V}(\mathcal{I}-\mathcal{O}_1+\mathcal{W})^{-1}(\mathcal{I}+\mathcal{O}_2)(\mathcal{I}-\mathcal{O}_2)^{-1}(\mathcal{I}+\mathcal{O}_1-\mathcal{W}). \tag{41}$$

$$\begin{pmatrix}
-O^{r-}_{1,1}-O^{r+}_{1,1} & 0 & 0 & 0 & O^{r+}_{1,1} & 0 & 0 & 0 & \\
0 & -O^{r-}_{1,2}-O^{r+}_{1,2} & 0 & 0 & 0 & O^{r+}_{1,2} & 0 & 0 & \\
0 & 0 & -O^{r-}_{1,3}-O^{r+}_{1,3} & 0 & 0 & 0 & O^{r+}_{1,3} & 0 & \\
0 & 0 & 0 & -O^{r-}_{1,4}-O^{r+}_{1,4} & 0 & 0 & 0 & 0 & \\
O^{r-}_{2,1} & 0 & 0 & 0 & -O^{r-}_{2,1}-O^{r+}_{2,1} & 0 & 0 & 0 & \cdots \\
0 & O^{r-}_{2,2} & 0 & 0 & 0 & -O^{r-}_{2,2}-O^{r+}_{2,2} & 0 & 0 & \\
0 & 0 & O^{r-}_{2,3} & 0 & 0 & 0 & -O^{r-}_{2,3}-O^{r+}_{2,3} & 0 & \\
0 & 0 & 0 & O^{r-}_{2,4} & 0 & 0 & 0 & -O^{r-}_{2,4}-O^{r+}_{2,4} & \\
 & & & & \vdots & & & & \ddots
\end{pmatrix}$$

FIG. 3. The $\mathcal{O}_r$ matrix for a 12-point (3×4) discretized domain in the two-dimensional spherical coordinate system, with $i \in [1,3]$ and $j \in [1,4]$. Depending on the boundary conditions, a few of the elements shown may become zeros.

Direct calculation of the $\mathcal{O}_d$ matrices for a few grids shows that this expression cannot be Hermitian when the field w is arbitrarily given and thus this ADI method cannot conserve the amount of material regardless of the use of the FVM.

The story is much more interesting when the simple ADI method is modified by adopting the operator splitting technique. Its matrix equation now changes to

$$(\mathcal{I}-\mathcal{O}_2)|q^{n+1/2}\rangle = (\mathcal{I}+\mathcal{O}_1)\mathcal{X}|q^n\rangle, \tag{42a}$$

$$(\mathcal{I}-\mathcal{O}_1)\mathcal{X}^{-1}|q^{n+1}\rangle = (\mathcal{I}+\mathcal{O}_2)|q^{n+1/2}\rangle. \tag{42b}$$

From these equations, one needs to check if the following matrix is Hermitian:

$$\mathcal{V}\mathcal{X}(\mathcal{I}-\mathcal{O}_1)^{-1}(\mathcal{I}+\mathcal{O}_2)(\mathcal{I}-\mathcal{O}_2)^{-1}(\mathcal{I}+\mathcal{O}_1)\mathcal{X}. \tag{43}$$

After some algebra (see Appendix C), the sufficient and necessary condition for the material conservation of the operator splitting ADI turns out to be

$$\mathcal{O}_2\mathcal{O}_1^2 = \mathcal{O}_1^2\mathcal{O}_2. \tag{44}$$

The operator algebra stops here and we need to directly compare the components of $\mathcal{O}_2\mathcal{O}_1^2$ and $\mathcal{O}_1^2\mathcal{O}_2$. Even though the full conditions for Eq. (44) are messy, one of them turns out to be the equation $O^{2+}_{i,j} + O^{2-}_{i,j} = O^{2+}_{i+1,j} + O^{2-}_{i+1,j}$. In the previously formulated FVM in the spherical coordinate system, $B^{\theta+}_{i,j} + B^{\theta-}_{i,j} \propto 1/(r_i^2 + \Delta r^2/12)$ varies with respect to i and the above equation cannot be satisfied; thus, even when the FVM with operator splitting is adopted, the ADI method fails to conserve material in the spherical coordinate system and the conclusion is the same for the cylindrical coordinate system. In the Cartesian coordinate system, however, our FVM satisfies Eq. (44), because the geometric factors for the flux calculation $B^{d\pm}_{\mathbf{i}}$ are independent of the position and the $\mathcal{O}_d$'s commute. Note that for the Cartesian coordinate system, the FDM can be made to be equal to our FVM and such an

$$\begin{pmatrix}
-O^{\theta-}_{1,1}-O^{\theta+}_{1,1} & O^{\theta+}_{1,1} & 0 & O^{\theta-}_{1,1} & 0 & 0 & 0 & 0 & \\
O^{\theta-}_{1,2} & -O^{\theta-}_{1,2}-O^{\theta+}_{1,2} & O^{\theta+}_{1,2} & 0 & 0 & 0 & 0 & 0 & \\
0 & O^{\theta-}_{1,3} & -O^{\theta-}_{1,3}-O^{\theta+}_{1,3} & O^{\theta+}_{1,3} & 0 & 0 & 0 & 0 & \\
O^{\theta+}_{1,4} & 0 & O^{\theta-}_{1,4} & -O^{\theta-}_{1,4}-O^{\theta+}_{1,4} & 0 & 0 & 0 & 0 & \\
0 & 0 & 0 & 0 & -O^{\theta-}_{2,1}-O^{\theta+}_{2,1} & O^{\theta+}_{2,1} & 0 & O^{\theta-}_{2,1} & \cdots \\
0 & 0 & 0 & 0 & O^{\theta-}_{2,2} & -O^{\theta-}_{2,2}-O^{\theta+}_{2,2} & O^{\theta+}_{2,2} & 0 & \\
0 & 0 & 0 & 0 & 0 & O^{\theta-}_{2,3} & -O^{\theta-}_{2,3}-O^{\theta+}_{2,3} & O^{\theta+}_{2,3} & \\
0 & 0 & 0 & 0 & O^{\theta+}_{2,4} & 0 & O^{\theta-}_{2,4} & -O^{\theta-}_{2,4}-O^{\theta+}_{2,4} & \\
 & & & & \vdots & & & & \ddots
\end{pmatrix}$$

FIG. 4. The $\mathcal{O}_\theta$ matrix for a 12-point (3×4) discretized domain in the two-dimensional spherical coordinate system, with $i \in [1,3]$ and $j \in [1,4]$. Depending on the boundary conditions, a few of the elements shown may become zeros.

FDM will guarantee material conservation when the operator splitting ADI method is adopted [22].

As mentioned earlier in this section, there are other known ADI methods [26,27]. In principle, each method must be independently tested for the material conservation and we performed a few such tests. Interestingly, we always obtain the same condition for the material conservation, Eq. (44), and it is okay to consider that the above conclusion holds true for most known ADI methods. One such analysis for a numerical scheme known as the Douglas-Gunn ADI method [10,22,28–30] is shown in Appendix D.

E. Material conservation of the SCFT with the higher-order FVM

In this section we describe the material conservation property of the SCFT adopting the higher-order finite-volume method. For the convenience of discussion, we restrict our analysis to the one-dimensional case. The general form of higher-order one-dimensional Laplacian can be written by the linear combination

$$\delta^2 f_i^n = \sum_k B_{i,k} f_k^n. \tag{45}$$

One natural constraint of $B_{i,k}$ is $\sum_k B_{i,k} = 0$, because $\delta^2 f_i^n$ must vanish for constant f_i^n. When the Crank-Nicolson method is adopted, the condition for the material conservation of the SCFT, $(\mathcal{VU})^\dagger = \mathcal{VU}$, still produces $(\mathcal{VO})^\dagger = \mathcal{VO}$ regardless of the use of higher-order schemes. With the current notation, this condition can be written as

$$B_{i,k}\Delta V_i - B_{k,i}\Delta V_k = 0. \tag{46}$$

The situation is somewhat different when higher-order schemes are adopted for the normal diffusion equation. For its analysis, let us temporarily adopt the following vector representation in which the cell volume ΔV_i and the function f_i^n are respectively written as

$$\begin{aligned}\mathbf{V} &= [\Delta V_1 \;\; \Delta V_2 \;\; \Delta V_3 \;\; \Delta V_4 \;\; \cdots \;\; \Delta V_I]^T,\\ \mathbf{f}_n &= [f_1^n \;\; f_2^n \;\; f_3^n \;\; f_4^n \;\; \cdots \;\; f_I^n]^T.\end{aligned} \tag{47}$$

For the case of the normal diffusion equation, f_i^n is the material density and the mass conservation condition at each time step is given as

$$\mathbf{V}^T\mathbf{f}_n = \mathbf{V}^T\mathbf{f}_{n+1} = \mathbf{V}^T\mathcal{U}\mathbf{f}_n. \tag{48}$$

In order to claim that a given numerical scheme conserves material, the above equation must be true regardless of the value of $\mathbf{f}_n$, which means that the row vector $\mathbf{V}^T$ must be a left eigenvector of the evolution matrix $\mathcal{U}$ with eigenvalue 1, that is, $\mathbf{V}^T\mathcal{U} = \mathbf{V}^T$. When $\mathcal{U}$ of the Crank-Nicolson method is used, it takes some algebra to show that this condition is equivalent to the equation $\sum_k B_{k,i}\Delta V_k = 0$. By using $B_{i,i} = -\sum_{k,k\neq i} B_{i,k}$, the above equation changes into $\sum_{k,k\neq i}[B_{i,k}\Delta V_i - B_{k,i}\Delta V_k] = 0$. Adding $B_{i,i}\Delta V_i - B_{i,i}\Delta V_i$ to both sides, it finally becomes

$$\sum_k [B_{i,k}\Delta V_i - B_{k,i}\Delta V_k] = 0. \tag{49}$$

This is the necessary and sufficient condition for the material conservation of the normal diffusion equation. Comparing this with Eq. (46), we conclude that a method which conserves material of the SCFT also conserves material of the normal diffusion equation, but the reverse is not always true.

The finite-volume method is formulated to conserve the amount of material of the normal diffusion problem, which means Eq. (49) is always satisfied regardless of the use of the higher-order schemes. In Sec. IV C we confirmed that the three-point FVM conserves material of the SCFT, but it remains to check the material conservation of the SCFT with higher-order schemes. In a general FVM, the Laplacian at point i is calculated from the flux differences as

$$\delta^2 f_i^n = \frac{F_{i+1/2} - F_{i-1/2}}{\Delta V_i}, \quad F_{i+1/2} = \sum_k C_{i+1/2,k} f_k^n, \tag{50}$$

where $C_{i+1/2,k}$ are numerical coefficients for the given FVM and they must satisfy $\sum_k C_{i+1/2,k} = 0$ to make $F_{i+1/2} = 0$ for constant f_i^n. Comparing them with Eq. (45), one can confirm that $B_{i,k} = (C_{i+1/2,k} - C_{i-1/2,k})/\Delta V_i$. Using Eq. (46),

$$C_{i+1/2,k} - C_{i-1/2,k} = C_{k+1/2,i} - C_{k-1/2,i} \tag{51}$$

is the condition for the material conservation of the SCFT. This equation must be true for every $i \in [1, I]$ and $k \in [1, I]$.

For the three-point FVM, most of the $C_{i\pm1/2,k}$ are zeros and we only need to check the two cases $k = i$ and $k = i + 1$. The case $k = i$ is trivially true, and when $k = i + 1$, Eq. (51) becomes $C_{i+1/2,i+1} = -C_{i+1/2,i}$. For the three-point FVM, $\sum_k C_{i+1/2,k} = 0$ is equivalent to this equation and the material conservation of the SCFT is again confirmed. The situation is different for higher-order FVM. Various formulations of higher-order FVM are available [24,32–34], but they do not satisfy Eq. (51) in general. This is one reason we recommend our three-point FVM for those who want to develop numerical SCFT algorithms adopting the FVM.

V. IRREGULAR GEOMETRY AND NUMERICAL RESULTS

In this section we upgrade our SCFT method to model two interesting nanostructured polymer systems in which polymers do not assemble into a regular geometry such as a rectangular parallelepiped, a cylinder, or a sphere. Since the polymer-filled region and the orthogonal coordinates do not perfectly match, the discretized Laplacian at the boundary cell, which has a fractional cell volume and surfaces, is calculated in a special way. Figure 5 exhibits a pictorial demonstration of the polymer-filled, partially filled, and empty cells in the orthogonal coordinate systems. The computation of the geometric factors $B_{\mathbf{i}}^{d\pm}$ must be conducted carefully depending on the cell and boundary shapes.

The geometric factors for the green dotted polymer-filled cells can be obtained by the FVM we formulated in Sec. III. For the actual calculation of $B_{\mathbf{i}}^{d\pm}$ in the three-dimensional cylindrical coordinate system [Fig. 5(b)], see Appendix A. The geometric factors for the red dotted empty cells are all zeros. A careful consideration is necessary for the yellow dotted partially filled cells. For these cells, the geometric factor at each boundary must be calculated directly from the definition (12b), using the actual fractional volume and surface area of the cell. One such example is marked by red lines in

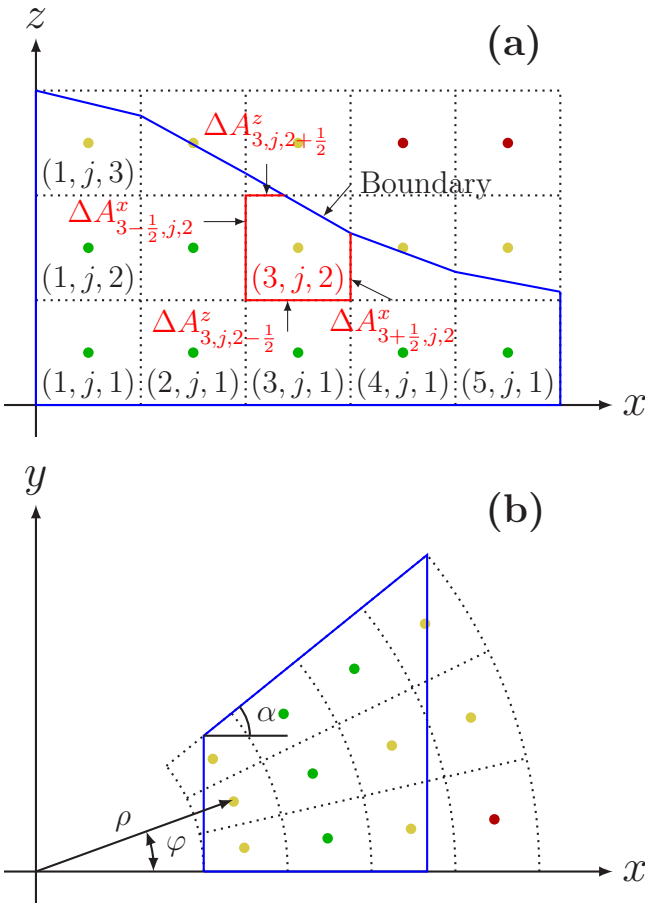

FIG. 5. Pictorial representation of orthogonal coordinates for polymers in irregular geometries. (a) Cartesian coordinate system with curved boundary. Cell $C_{3,j,2}$ is highlighted with red lines as an example. In the y direction, the two-dimensional slice at the jth cells is shown. (b) Cylindrical coordinate system modeling a thin film with thickness variation. The slope of the upper surface is α. In the z direction, the two-dimensional slice is shown. Green dotted cells have the whole volumes and yellow dotted cells have only fractional volumes. Red dotted cells are skipped in the calculation because no flux flows in or out of the cells.

Fig. 5(a). Note that no flux passes through the irregular system boundary marked by blue lines. After this modification, we calculate the evolution of the partial partition functions using the three-dimensional operator splitting Douglas-Gunn ADI method (see Appendix D).

For the first example, we study the alignment of symmetric AB diblock copolymer domains in the thickness-modulated region confined by surfaces curved in one direction. This subject was inspired by the experimental work of Kim *et al.* [35], which reported that the thickness modulation promotes the alignment of lamellar domains. In order to implement the numerical SCFT in this geometry, we choose the Cartesian coordinate system adopting fractional cells at the polymer-air boundary. The simplified demonstration of this coordinate system is shown in Fig. 5(a). Since the film has a reflection symmetry along the y-z plane, we restrict our calculation to the right half of the film shown in experiments. For the convenience of cell volume calculation, the curved surface on a cell is approximated by a planar surface as shown in Fig. 5(a).

In our model, the film consists of n_p symmetric incompressible AB diblock copolymers with the A fraction $f = 0.5$. The Flory-Huggins parameter for the AB interaction is chosen to be $\chi N = 20$ and each polymer is considered as a Gaussian chain whose natural end-to-end length is $aN^{1/2}$. We omit the derivation of equations here and only present the result (see Ref. [2] for the details). The mean fields acting on A and B blocks are given as

$$w_A(\mathbf{r}) = \chi N \phi_B(\mathbf{r}) + \xi(\mathbf{r}), \tag{52a}$$

$$w_B(\mathbf{r}) = \chi N \phi_A(\mathbf{r}) + \xi(\mathbf{r}), \tag{52b}$$

where $\phi_A(\mathbf{r})$ and $\phi_B(\mathbf{r})$ are the ensemble-average segment concentration of A and B blocks, respectively, and $\xi(\mathbf{r})$ is the pressure field. The mean field free energy per chain is

$$\frac{F}{n_p k_B T} = -\ln\left(\frac{Q}{V_{\text{tot}}}\right) + \frac{1}{V_{\text{tot}}}\int d\mathbf{r}[\chi N \phi_A(\mathbf{r})\phi_B(\mathbf{r}) - w_A(\mathbf{r})\phi_A(\mathbf{r}) - w_B(\mathbf{r})\phi_B(\mathbf{r})], \tag{53}$$

where Q is the total partition function of the diblock copolymers and V_{tot} is the polymer-filled system volume. At $\chi N = 20$, the natural lamellar domain period is $L_0 = 1.643aN^{1/2}$, and we assign the computation box size of $20L_0 \times 20L_0 \times 4L_0$, which is represented by a Cartesian grid of $300 \times 300 \times 60$, and $\Delta s = 0.02$ is used. For the modeling of the thickness variation of the film, the height of the polymer-air surface is given as a curved function $L_z(x,y) = (4L_0/aN^{1/2})\exp(-x^2/98a^2N) \times (4L_0 - 1.2aN^{1/2}) + 1.2aN^{1/2}$. The polymer chains reside only under the curved surface.

In order to investigate the preferred direction of the lamellar domain alignment, our SCFT computation is conducted with the initial condition that the lamellar domains are aligned in the x, y, or z direction. The results are shown in Fig. 6 and we can see that each morphology aligned in the x, y, or z direction is at least metastable. Note that the z-directionally aligned domains exhibit local kinks and distortions to fit into the curved system geometry, which was also observed in previous theoretical works [18,36].

We compare the free energy of each phase for the determination of the stable morphology. The free energy of the z-directionally aligned phase is $4.0303k_BT$ per chain, which is much higher than the other two cases. It can be easily attributed to the incommensurability of the film thickness and the presence of the kinks and distortions. The y-directionally aligned phase has a free energy of $3.9829k_BT$ per chain, which is slightly below that of the x-directionally aligned phase, $3.9844k_BT$. The difference $0.0015k_BT$ is small but meaningful in our calculation using fine grid and it clearly suggests that the preferable morphology is the y-directionally aligned one. This result is consistent with the conclusion of the experimental work [35] which suggested that this alignment is due to the tendency to minimize elastic energy in the irregular geometry of confinement. For the x-directionally aligned morphology, the lamellae tend to be aligned perpendicular to both the top and bottom surfaces, but it inevitably bends the layers, which costs additional free energy. In Ref. [35]

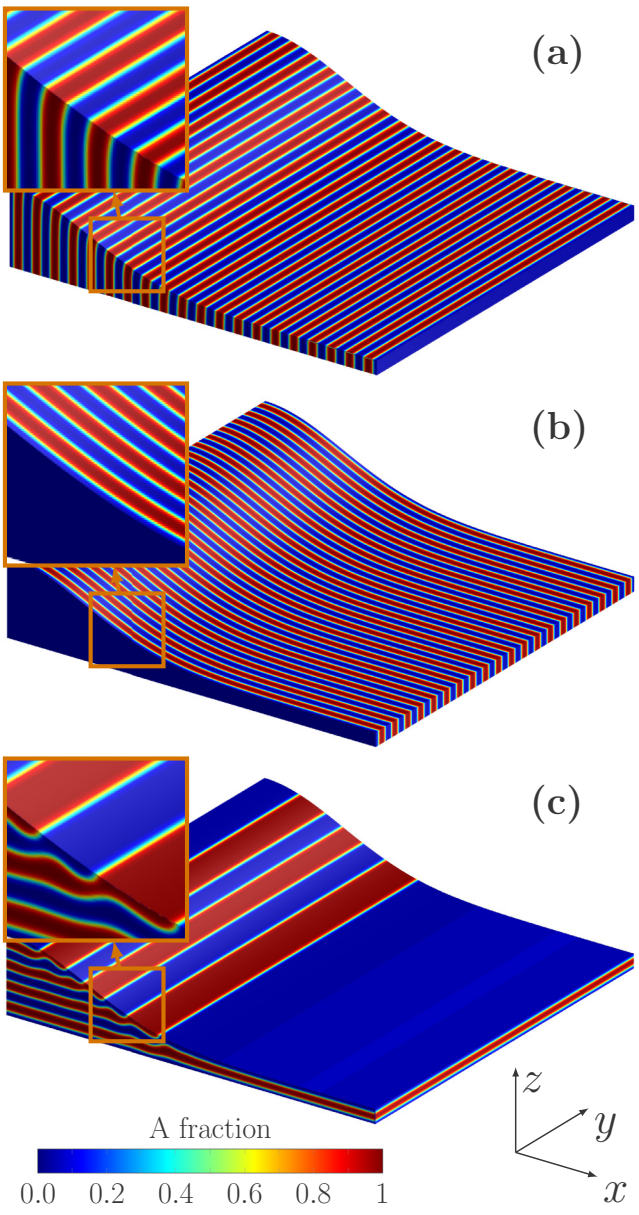

FIG. 6. Possible AB diblock copolymer morphologies in a thickness-modulated geometry. The segment concentrations of the A block (ϕ_A) and the B block (ϕ_B) are shown in red and blue, respectively. The lamellae are aligned in the (a) x, (b) y, and (c) z directions.

this thickness-modulation promoted alignment mechanism is called geometrical anchoring.

Our second example is an asymmetric ($f = 0.3$) incompressible diblock copolymer thin film with linear thickness variation. A similar problem was the subject of Ref. [37]. We choose $\chi N = 18$, which produces a cylindrical phase with a natural cylinder-to-cylinder distance $L_0 = 1.638aN^{1/2}$. The film is now trapezoid shaped, as shown in Fig. 5(b) with exaggeration. In order to apply a surface interaction on the top and bottom surfaces [37], we perform the SCFT calculation in the cylindrical coordinate system in which the cell boundaries naturally follow the thin film surfaces as shown in the figure.

The film thickness varies from $0.200L_0$ to $2.000L_0$ in a lateral length of $31.443L_0$ and the width of the film is $3.500L_0$. With the choice of $\Delta\rho = 0.082aN^{1/2}$, $\Delta\varphi = 1.429 \times 10^{-3}$ rad, and $\Delta z = 0.082aN^{1/2}$, the simulation is conducted on a grid of $630 \times 40 \times 70$. The preference of the A block to the air is represented by the parameter η_A [10,18,22], so the mean field acting on each segment is written in the cylindrical coordinate system as

$$w_A(\mathbf{r}) = \chi N\phi_B(\mathbf{r}) + \xi(\mathbf{r}) - \frac{2\eta_A}{\rho}[\delta(\varphi) + \delta(\varphi - \alpha)]aN^{1/2}, \tag{54a}$$

$$w_B(\mathbf{r}) = \chi N\phi_A(\mathbf{r}) + \xi(\mathbf{r}), \tag{54b}$$

where α is the slope of the surface as shown in Fig. 5(b) and we choose $\alpha = 5.717 \times 10^{-2}$ rad (3.276°) for the current simulation.

Figure 7 shows the result of a few simulations with different η_A. In the absence of interfacial energy, cylindrical domains parallel to the film surface are preferable only when the thickness of the film is specially chosen to be commensurate with them. For the current system with thickness variation, commensurability cannot always be satisfied and short cylinders perpendicular to the surface are usually chosen for the thin part of the film as shown in Fig. 7(a). As the film thickness increases, the influence of confinement on the overall alignment decreases and cylinders with mixed orientations are observed on the right-hand side of the figure.

The situation changes when the top and bottom surfaces prefer one block over the other. Figure 7(b) shows the case that the surfaces prefer the minority block, while Fig. 7(c) corresponds to the opposite case. For Fig. 7(b) the region with vertical cylinders is much narrower than the neutral case, because domain A tends to stick to the top and bottom surfaces. This tendency creates a single-layer lamellar phase as the film thickness increases. At the thicker region, surface-parallel cylinders are observed and they are eventually interconnected to form a bicontinuous phase.

The region with vertical cylinders is also narrow for Fig. 7(c) because domain A now tends to stay in the interior. As the film thickness increases, the vertical cylinders gradually become spherical and then surface-parallel cylinders appear. At the thicker region, they are interconnected and form a perforated lamellar phase and it eventually becomes multilayered.

One may be tempted to solve these problems by introducing nonorthogonal skewed coordinates which follow the exact shape of the polymeric system. However, such attempts usually require a complicated numerical implementation. Moreover, it can only be achieved by the sacrifice of speed because discretization of the Laplacian in the nonorthogonal coordinates cannot be calculated from the information of nearest cells, which limits the use of the ADI method.

For Fig. 6 we are using the operator splitting ADI method in the Cartesian coordinate system, which in principle preserves material perfectly. However, the presence of fractional cells at the system boundary makes $B_{\mathbf{i}}^{d\pm}$ dependent on the position, which breaks the material preservation slightly. For the second example, use of the operator splitting ADI method in the

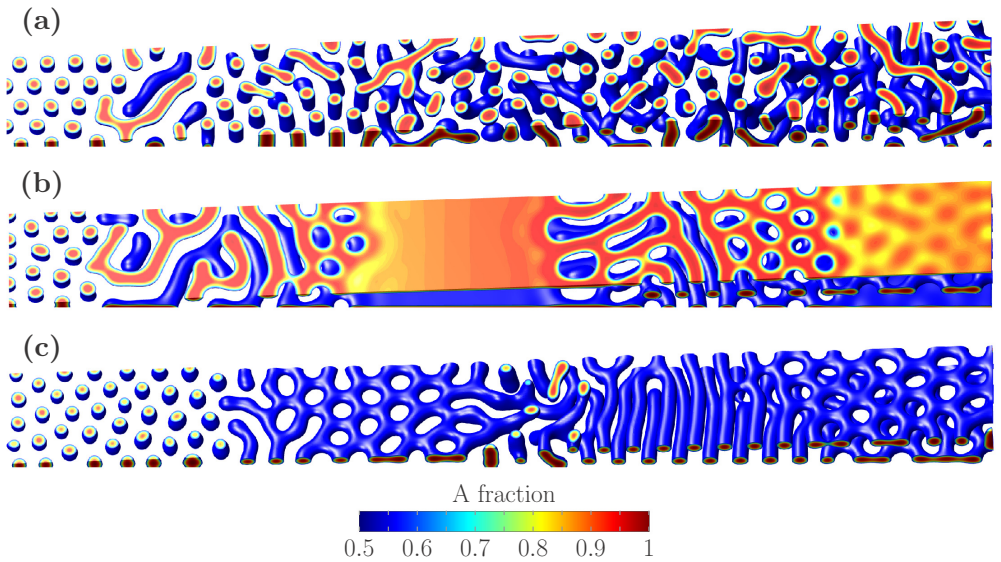

FIG. 7. Simulation of AB block copolymers in a large thickness-modulated film with surface interaction (a) $\eta_A = 0$, (b) $\eta_A = 0.2$, and (c) $\eta_A = -0.3$. For clarification, only the regions with $\phi_A \geqslant 0.5$ are shown with colors.

cylindrical coordinate system breaks the material preservation even before introducing fractional cells. Despite this, with the application of the FVM formulated in this paper, we can manage to keep the error level low enough to distinguish competing morphologies. For the two systems, the relative errors defined by $\sum_{\mathbf{i}}(\phi^A_{\mathbf{i}} + \phi^B_{\mathbf{i}} - 1)\Delta V_{\mathbf{i}}/V_{\text{tot}}$ vary from 10^{-6} to 10^{-10}, depending on the parameters chosen.

For a systematic test of the free energy convergence, we take an example of block copolymers with $f = 0.25$ and $\chi N = 18$, which are known to form a body-centered-cubic (bcc) phase in bulk with the unit cell size $1.86aN^{1/2}$. Our target must be a known but nontrivial morphology and thus we use a box with varying thickness, as shown in Fig. 5(b). We choose the system shape to be close to the original bcc unit cell with a height variation of 20%. The natural choice is $L_z = 1.86aN^{1/2}$, the inner radius $\rho_{1/2} = 9.30aN^{1/2}$, and the outer radius $\rho_{I+1/2} = 11.16aN^{1/2}$. The angle φ varies from 0 to 0.182 rad to make the arc length at the central region $1.86aN^{1/2}$.

Because of the fractional cells in the system, implementing an FDM adopting the ADI method is rather difficult and we compare the FVM with the operator splitting ADI method [FVM(OS)] and the FVM without the operator splitting ADI method [FVM(non-OS)] in this analysis. To reduce the number of free parameters, we set $I = J = K$, with I varying from 40 to 80, and $1/\Delta s$ up to 700 is used. The equilibrium morphology at $I = 80$ and $1/\Delta s = 700$ is shown in Fig. 8(a) and the distorted bcc structure is found, as expected. The free energy convergence is shown in Fig. 8(b). It is observed that at a given I value, both the FVM(OS) and FVM(non-OS) converge to a certain free energy as $1/\Delta s$ increases and the convergence is better for the FVM(OS). As I increases, the converging free energy approaches to the actual free energy drawn by a dotted line. At $I = 80$ and $1/\Delta s = 200$, the free energy convergence of the FVM(OS) is excellent, but the FVM(non-OS) can achieve such an accuracy only at $1/\Delta s = 700$.

The mass errors are found to behave in a slightly different way. The error depends weakly on the I value and thus it is enough to describe its $1/\Delta s$ dependence here. For the FVM(non-OS), the mass error was above 10^{-5} at $1/\Delta s = 100$ and it reduces to 10^{-6} at $1/\Delta s = 700$. The FVM(OS) can achieve 10^{-6} of error at $1/\Delta s = 100$ and it can go below 10^{-9} at $1/\Delta s = 700$. This analysis suggests that our choice of the FVM(OS) for the problems of Figs. 6 and 7 is appropriate and the free energy differences reported for Fig. 6 are meaningful.

Our method using the FVM and the ADI method is in principle as fast as any existing SCFT methods with high resolution. The only complication comes in the implementation of the FVM, which is a one-time upgrade from the FDM after the required equations are derived. Consider a given mesh with points $M = I \times J \times K$. For each contour step Δs, multiplication of $\mathcal{X}$ takes time $O(M)$ and it takes another time $O(M)$ to solve the tridiagonal matrix equations. Thus, the overall time complexity becomes $O(M/\Delta s)$ [38]. One additional advantage of this method is that parallelization of the algorithm is easy with high parallel efficiency. For our first example, with the use of 15 cores of Xeon Gold 6132 CPUs and the OpenMP library, one iteration takes 12 s. Up to 10 000 iterations are necessary for the stabilization of the global morphology, but the whole calculation is usually completed within a day.

VI. DISCUSSION AND CONCLUSION

We have successfully developed an algebraic test verifying the material conservation of the numerical SCFT. By introducing the bra-ket notation, the condition for the material conservation turns out to be equivalent to $(\mathcal{V}\mathcal{U})^\dagger = \mathcal{V}\mathcal{U}$, where $\mathcal{V}$ and $\mathcal{U}$ are the volume and evolution operators, respectively. Using this method, we have proven that the material conservation is perfect for the pseudospectral method in the Cartesian grid, which is the most widely used SCFT numerical scheme nowadays.

The situation is more complicated when the SCFT real-space methods using the FDM or FVM are adopted. For

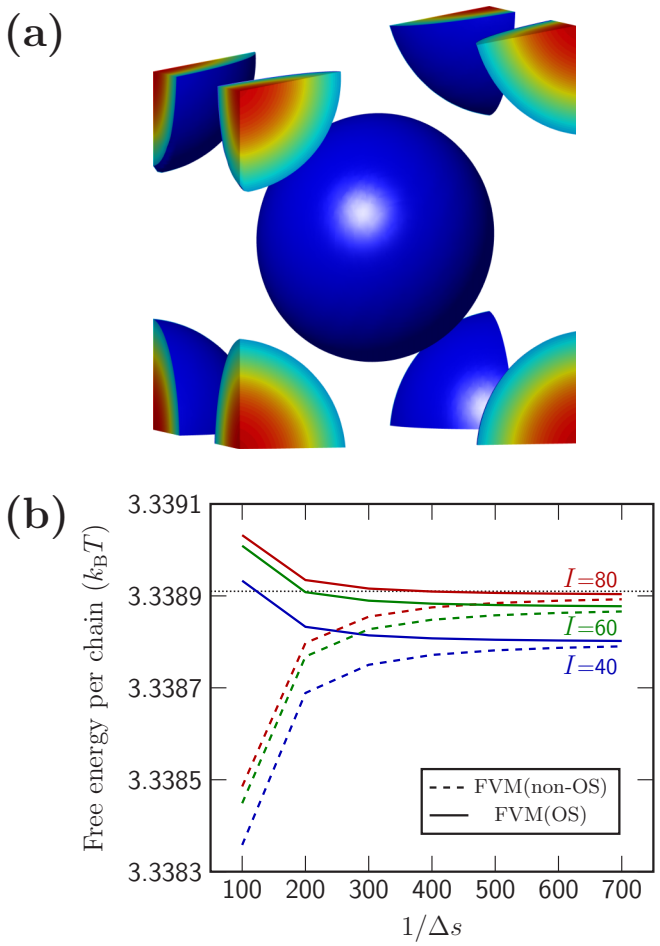

FIG. 8. Convergence and error analysis for the cylindrical grid in Fig. 5(b). (a) Distorted bcc morphology observed for block copolymers with $f = 0.25$ and $\chi N = 18$, inside a box with varying thickness. (b) The FVM free energies at various $I = J = K$ values plotted as functions of $1/\Delta s$. The FVM(OS) (solid lines) and FVM(non-OS) (dashed lines) are shown along with our best estimation for the free energy drawn with a dotted line [FVM(OS), with $I = 250$ and $1/\Delta s = 700$].

the Crank-Nicolson method, the material conservation requirement is $(\mathcal{V}\mathcal{O})^\dagger = \mathcal{V}\mathcal{O}$, where $\mathcal{O}$ is the rescaled discrete Laplacian operator. In the three-point approximation, this condition is always satisfied regardless of the coordinate system when the Laplacian in the modified diffusion equation is discretized by the FVM. The three-point FDM is equivalent to the FVM in the Cartesian coordinate system and thus the material conservation is trivial. However, the FDM and FVM are not the same for other coordinate systems such as the cylindrical and spherical coordinate systems and three-point FDM fails to conserve material for them. The discretization of the SCFT using the finite-volume approach in the generic orthogonal coordinate system was explained in Sec. III and its explicit application in the spherical and cylindrical coordinate systems was provided in the same section and Appendix A.

The FVM is designed to conserve material for the normal diffusion problem, but the analysis at the end of Sec. IV showed that not all FVMs conserve material when they are adopted by the SCFT. Various formulations of higher-order FVMs are available, but they are not designed to conserve material for the SCFT. For example, our tests of higher-order FVMs using reconstruction schemes such as the weighted essentially nonoscillatory scheme [32,33] and piecewise parabolic method [24,34] reveal that they are inappropriate for the the SCFT. Because of this, we recommend the three-point FVM formulated in this paper for the SCFT applications.

In order to solve parabolic problems efficiently, ADI methods are often used as an approximation of the Crank-Nicolson method. By applying the same algebraic test to various ADI methods, we have shown that the FVM in the cylindrical and spherical coordinate systems cannot conserve material. The FVM in the Cartesian coordinate system is special in that the use of the operator splitting ADI method conserves material and this is the only known ADI method that conserves material for the SCFT.

In short, the amount of material is conserved for the SCFT when the following numerical methods are adopted: (i) the pseudospectral method in the Cartesian coordinate system, (ii) the Crank-Nicolson method with the FVM, and (iii) the operator splitting ADI method with the FVM in the Cartesian coordinate system. Note that for the two polymeric systems we investigated in this paper, we adopt operator splitting ADI methods with the FVM. Even though their material conservation is not perfect, the error is reduced significantly by the adoption of the FVM, and the ADI method with the FVM is a recommendable choice for most practical polymeric systems as a compromise between speed and accuracy.

By introducing fractional cells in the FVM formulation, accurate SCFT calculations have been performed for systems with irregular geometry. Our first system is the symmetric ($f = 0.5$) incompressible AB diblock copolymers residing in a thickness-modulated region confined by surfaces curved in one direction. By comparing free energies of the candidate phases, it has been found that the block domains tend to be aligned in a direction perpendicular to both surfaces. This morphology is consistent with the experimental report of Kim *et al.* [35].

Our second example is the asymmetric ($f = 0.3$) incompressible AB diblock copolymer thin film with linear thickness variation. We have performed the SCFT calculation by applying a surface interaction on the top and bottom surfaces. In the absence of interfacial energy, short upright cylinders are observed for the thinnest part of the film. As the film thickness increases, cylinders with mixed orientations are observed. When both surfaces prefer either the minority or the majority block, at the thicker part of the film, the minority domains are interconnected and they eventually form perforated lamellar or multilayered phase. By analyzing the free energy convergence and the mass conservation error, we have shown that a very accurate and fast SCFT calculation is possible with the choice of the FVM with the operator splitting ADI method.

ACKNOWLEDGMENTS

This research was supported by Basic Science Research Program through the National Research Foundation of Korea funded by the Ministry of Science, ICT & Future Planning (Grants No. 2014R1A2A1A11054430 and No. 2017R1A2B4012377). This research used high performance computing resources of the UNIST Supercomputing Center.

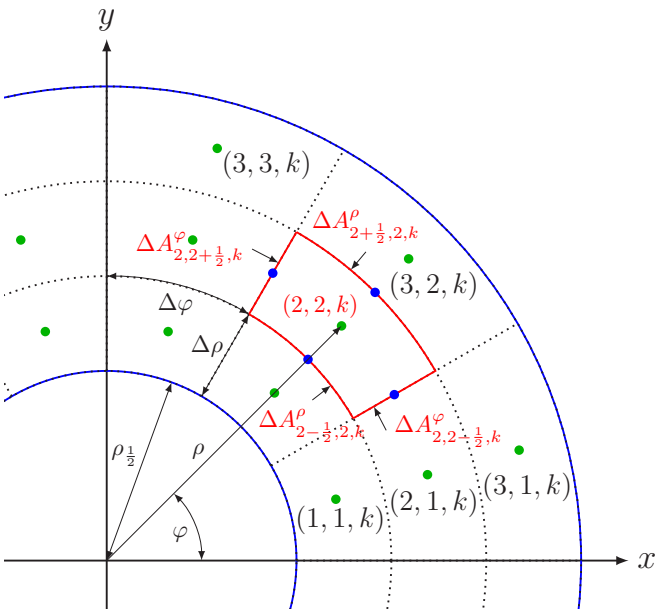

FIG. 9. Pictorial representation of the discretized cylindrical coordinate system, for the case of $I = 3$, $J = 12$, $\rho_{1/2} = 2\Delta\rho$, and $\Delta\varphi = \pi/6$. In the z direction, the two-dimensional slice at the kth cells is shown. The system boundary is at $\rho_{\frac{1}{2}} = 2\Delta\rho$ and $\rho_{3+1/2} = 5\Delta\rho$ in the ρ direction and there is a periodic boundary in the φ direction so that $\varphi_{1/2} = 0$ is equivalent to $\varphi_{12+1/2} = 2\pi$. Each green dot represents a grid point (i,j,k) and the neighboring region surrounded by dotted lines indicates the grid cell $C_{i,j,k}$. The cell $C_{2,2,k}$ is highlighted with red lines as an example. Each blue dot denotes the midpoint of a surface where the scale factor for the gradient calculation must be selected.

APPENDIX A: THREE-DIMENSIONAL FINITE-VOLUME METHOD IN A CYLINDRICAL COORDINATE SYSTEM

In this appendix, using the generic FVM formulated in Sec. III, the discrete Laplacian operator for the cylindrical coordinate system is derived. In this coordinate system, the variables are $(x_1,x_2,x_3) = (\rho,\varphi,z)$ and the scale factors are $(h_1,h_2,h_3) = (1,\rho,1)$. The grid points and cell boundaries are illustrated in Fig. 9. Note that (ρ_i,φ_j,z_k) represents the point $(\rho_{\frac{1}{2}} + (i-\frac{1}{2})\Delta\rho,(j-\frac{1}{2})\Delta\varphi,(k-\frac{1}{2})\Delta z)$.

The areas of the two surfaces of cell $C_{\mathbf{i}}$ perpendicular to the vector $\hat{\mathbf{e}}_\rho$ are

$$\Delta A^{\rho}_{i\pm1/2,j,k} = \int_{z_{k-1/2}}^{z_{k+1/2}} \int_{\varphi_{j-1/2}}^{\varphi_{j+1/2}} \rho_{i\pm1/2} d\varphi\, dz = \rho_{i\pm1/2}\Delta\varphi\Delta z \tag{A1}$$

and the surface areas perpendicular to $\hat{\mathbf{e}}_\varphi$ and $\hat{\mathbf{e}}_z$ are

$$\Delta A^{\varphi}_{i,j\pm1/2,k} = \int_{z_{k-1/2}}^{z_{k+1/2}} \int_{\rho_{i-1/2}}^{\rho_{i+1/2}} d\rho\, dz = \Delta\rho\Delta z, \tag{A2}$$

$$\Delta A^{z}_{i,j,k\pm1/2} = \int_{\varphi_{j-1/2}}^{\varphi_{j+1/2}} \int_{\rho_{i-1/2}}^{\rho_{i+1/2}} \rho\, d\rho\, d\varphi = \frac{1}{2}\left(\rho^2_{i+1/2} - \rho^2_{i-1/2}\right)\Delta\varphi = \rho_i\Delta\rho\Delta\varphi. \tag{A3}$$

The volume of the cell $C_{i,j,k}$ is

$$\Delta V_{i,j,k} = \int_{z_{k-1/2}}^{z_{k+1/2}} \int_{\varphi_{j-1/2}}^{\varphi_{j+1/2}} \int_{\rho_{i-1/2}}^{\rho_{i+1/2}} \rho\, d\rho\, d\varphi\, dz = \frac{1}{2}\left(\rho^2_{i+1/2} - \rho^2_{i-1/2}\right)\Delta\varphi\Delta z = \rho_i\Delta\rho\Delta\varphi\Delta z. \tag{A4}$$

Using these equations and the scale factors $(h^{\rho\pm}_{i,j,k},h^{\varphi\pm}_{i,j,k},h^{z\pm}_{i,j,k}) = (1,\rho_i,1)$, one can obtain $B^{d\pm}_{\mathbf{i}}$, the geometric factors for the flux calculation,

$$B^{\rho\pm}_{i,j,k} = \frac{\Delta A^{\rho}_{i\pm1/2,j,k}}{h^{\rho\pm}_{i,j,k}\Delta\rho\Delta V_{i,j,k}} = \frac{\rho_{i\pm1/2}}{\rho_i\Delta\rho^2}, \tag{A5a}$$

$$B^{\varphi\pm}_{i,j,k} = \frac{\Delta A^{\varphi}_{i,j\pm1/2,k}}{h^{\varphi\pm}_{i,j,k}\Delta\varphi\Delta V_{i,j,k}} = \frac{1}{\rho_i^2\Delta\varphi^2}, \tag{A5b}$$

$$B^{z\pm}_{i,j,k} = \frac{\Delta A^{z}_{i,j,k\pm1/2}}{h^{z\pm}_{i,j,k}\Delta z\Delta V_{i,j,k}} = \frac{1}{\Delta z^2}. \tag{A5c}$$

Inserting these expressions in Eq. (12a) completes the calculation of the discrete Laplacian operator.

APPENDIX B: REMOVAL OF $\mathcal{X}$ MATRICES IN THE HERMITICITY PROOF

For the evolution operator of operator splitting schemes, the diagonal matrix $\mathcal{X} \equiv \exp(-\mathcal{W})$ is required and its components are $\mathcal{X}_{ii} = \exp(-\mathcal{W}_{ii})$. Our task is to check the Hermiticity of the matrix $\mathcal{V}\mathcal{X}\mathcal{A}\mathcal{X}$, where $\mathcal{A}$ is a generic evolution operator without fields. If $\mathcal{V}\mathcal{X}\mathcal{A}\mathcal{X}$ is Hermitian, the following equation holds true:

$$\mathcal{V}\mathcal{X}\mathcal{A}\mathcal{X} = \mathcal{X}\mathcal{A}^\dagger\mathcal{X}\mathcal{V}. \tag{B1}$$

Since $\mathcal{V}$ and $\mathcal{X}$ are diagonal, they commute and the above equation is equivalent to

$$\mathcal{X}\mathcal{V}\mathcal{A}\mathcal{X} = \mathcal{X}\mathcal{A}^\dagger\mathcal{V}\mathcal{X}. \tag{B2}$$

The matrix $\mathcal{X}$ is invertible, because $\mathcal{X}_{ii}$ is always nonzero. By multiplying $\mathcal{X}^{-1}$ once from the left and once from the right, we obtain

$$\mathcal{V}\mathcal{A} = \mathcal{A}^\dagger\mathcal{V}. \tag{B3}$$

Thus, the matrix $\mathcal{V}\mathcal{X}\mathcal{A}\mathcal{X}$ is Hermitian if and only if the matrix $\mathcal{V}\mathcal{A}$ is Hermitian. This theorem is useful for the Hermiticity check of an expression containing two $\mathcal{X}$ matrices.

APPENDIX C: ALTERNATING DIRECTION IMPLICIT METHOD

The ADI method [18,21,31] with operator splitting is

$$\left(1 - a^2N\frac{\Delta s}{12}\delta_2^2\right)q^{n+1/2}_{i,j} = \left(1 + a^2N\frac{\Delta s}{12}\delta_1^2\right)\exp\left(-\frac{\Delta s}{2}w_{i,j}\right)q^{n}_{i,j}, \tag{C1a}$$

$$\left(1 - a^2N\frac{\Delta s}{12}\delta_1^2\right)\exp\left(\frac{\Delta s}{2}w_{i,j}\right)q^{n+1}_{i,j} = \left(1 + a^2N\frac{\Delta s}{12}\delta_2^2\right)q^{n+1/2}_{i,j}. \tag{C1b}$$

Its bra-ket equation becomes

$$(\mathcal{I}-\mathcal{O}_2)|q^{n+1/2}\rangle = (\mathcal{I}+\mathcal{O}_1)\mathcal{X}|q^n\rangle,$$
$$(\mathcal{I}-\mathcal{O}_1)\mathcal{X}^{-1}|q^{n+1}\rangle = (\mathcal{I}+\mathcal{O}_2)|q^{n+1/2}\rangle. \quad \text{(C2)}$$

From these equations, the evolution operator is

$$\mathcal{U} = \mathcal{X}(\mathcal{I}-\mathcal{O}_1)^{-1}(\mathcal{I}+\mathcal{O}_2)(\mathcal{I}-\mathcal{O}_2)^{-1}(\mathcal{I}+\mathcal{O}_1)\mathcal{X} \quad \text{(C3)}$$

and we need to check if the following matrix is Hermitian:

$$\mathcal{V}\mathcal{X}(\mathcal{I}-\mathcal{O}_1)^{-1}(\mathcal{I}+\mathcal{O}_2)(\mathcal{I}-\mathcal{O}_2)^{-1}(\mathcal{I}+\mathcal{O}_1)\mathcal{X}. \quad \text{(C4)}$$

Before proceeding, we will construct a few useful equations which are valid when $\mathcal{O}_d$ matrix for the FVM is used. In this case, $\mathcal{O}_d\mathcal{V}^{-1}$ is Hermitian for each d, because each equation identifying the Hermiticity reduces to Eq. (37), which we confirmed for the FVM. Using this property, the following two equations can be confirmed:

$$\mathcal{V}(\mathcal{I}\pm\mathcal{O}_d)\mathcal{V}^{-1} = (\mathcal{I}\pm\mathcal{O}_d)^\dagger, \quad \text{(C5a)}$$
$$\mathcal{V}(\mathcal{I}-\mathcal{O}_d)^{-1}\mathcal{V}^{-1} = [(\mathcal{I}-\mathcal{O}_d)^{-1}]^\dagger, \quad \text{(C5b)}$$

where we assume that $\mathcal{I}-\mathcal{O}_d$ is invertible.

Using the theorem in Appendix B, the two $\mathcal{X}$ matrices in the evolution matrix are removable in checking the Hermiticity of the matrix. Starting from this modification of Eq. (C4),

$$\begin{aligned}
&\mathcal{V}(\mathcal{I}-\mathcal{O}_1)^{-1}(\mathcal{I}+\mathcal{O}_2)(\mathcal{I}-\mathcal{O}_2)^{-1}(\mathcal{I}+\mathcal{O}_1)\\
&\quad=\mathcal{V}(\mathcal{I}-\mathcal{O}_1)^{-1}[2\mathcal{I}-(\mathcal{I}-\mathcal{O}_2)](\mathcal{I}-\mathcal{O}_2)^{-1}(\mathcal{I}+\mathcal{O}_1)\\
&\quad=\mathcal{V}\{(\mathcal{I}-\mathcal{O}_1)^{-1}[2(\mathcal{I}-\mathcal{O}_2)^{-1}-\mathcal{I}](\mathcal{I}+\mathcal{O}_1)\}\\
&\quad=\mathcal{V}[2(\mathcal{I}-\mathcal{O}_1)^{-1}(\mathcal{I}-\mathcal{O}_2)^{-1}(\mathcal{I}+\mathcal{O}_1)\\
&\qquad-(\mathcal{I}-\mathcal{O}_1)^{-1}(\mathcal{I}+\mathcal{O}_1)]\\
&\quad=\mathcal{V}[2(\mathcal{I}-\mathcal{O}_1)^{-1}(\mathcal{I}-\mathcal{O}_2)^{-1}(\mathcal{I}+\mathcal{O}_1)\\
&\qquad-2(\mathcal{I}-\mathcal{O}_1)^{-1}+\mathcal{I}]. \quad \text{(C6)}
\end{aligned}$$

Using Eq. (C5b), $\mathcal{V}(\mathcal{I}-\mathcal{O}_1)^{-1}$ is Hermitian and the second and third terms can be removed in checking the Hermiticity of the matrix. After dividing by 2, what now remains to check is

$$\mathcal{V}(\mathcal{I}-\mathcal{O}_1)^{-1}(\mathcal{I}-\mathcal{O}_2)^{-1}(\mathcal{I}+\mathcal{O}_1). \quad \text{(C7)}$$

Using Eqs. (C5), the conjugate transpose of Eq. (C7) turns out to be equivalent to

$$\begin{aligned}
&(\mathcal{I}+\mathcal{O}_1)^\dagger[(\mathcal{I}-\mathcal{O}_2)^{-1}]^\dagger[(\mathcal{I}-\mathcal{O}_1)^{-1}]^\dagger\mathcal{V}\\
&\quad=\mathcal{V}(\mathcal{I}+\mathcal{O}_1)(\mathcal{I}-\mathcal{O}_2)^{-1}(\mathcal{I}-\mathcal{O}_1)^{-1}. \quad \text{(C8)}
\end{aligned}$$

Our task is to compare Eq. (C7) with Eq. (C8). Multiplying $(\mathcal{I}-\mathcal{O}_2)(\mathcal{I}-\mathcal{O}_1)\mathcal{V}^{-1}$ from the left and $(\mathcal{I}-\mathcal{O}_1)(\mathcal{I}-\mathcal{O}_2)$ from the right of both expressions, we get the condition

$$(\mathcal{I}-\mathcal{O}_2)(\mathcal{I}-\mathcal{O}_1)(\mathcal{I}+\mathcal{O}_1) = (\mathcal{I}+\mathcal{O}_1)(\mathcal{I}-\mathcal{O}_1)(\mathcal{I}-\mathcal{O}_2). \quad \text{(C9)}$$

Expanding this equation, the final sufficient and necessary condition for the material conservation of the operator splitting ADI with the FVM is

$$\mathcal{O}_2\mathcal{O}_1^2 = \mathcal{O}_1^2\mathcal{O}_2. \quad \text{(C10)}$$

For two arbitrary matrices $\mathcal{A}$ and $\mathcal{B}$, if $\mathcal{A}\mathcal{B}=\mathcal{B}\mathcal{A}$ is satisfied, $\mathcal{A}\mathcal{B}^2=\mathcal{B}^2\mathcal{A}$ is always true. Therefore,

$$\mathcal{O}_2\mathcal{O}_1 = \mathcal{O}_1\mathcal{O}_2 \quad \text{(C11)}$$

is a sufficient condition for Eq. (C10). The two matrices $\mathcal{O}_1$ and $\mathcal{O}_2$ are sparse and the matrix multiplication can be performed. The requirements for Eq. (C11) turn out to be

$$O^{1+}_{i,j} + O^{1-}_{i,j} - O^{1+}_{i,j+1} - O^{1-}_{i,j+1} = 0, \quad \text{(C12a)}$$
$$O^{2+}_{i,j} + O^{2-}_{i,j} - O^{2+}_{i+1,j} - O^{2-}_{i+1,j} = 0, \quad \text{(C12b)}$$
$$O^{1-}_{i,j}O^{2-}_{i-1,j} - O^{1-}_{i,j-1}O^{2-}_{i,j} = 0, \quad \text{(C12c)}$$
$$O^{1-}_{i,j}O^{2+}_{i-1,j} - O^{1-}_{i,j+1}O^{2+}_{i,j} = 0, \quad \text{(C12d)}$$
$$O^{1+}_{i,j}O^{2-}_{i+1,j} - O^{1+}_{i,j-1}O^{2-}_{i,j} = 0, \quad \text{(C12e)}$$
$$O^{1+}_{i,j}O^{2+}_{i+1,j} - O^{1+}_{i,j+1}O^{2+}_{i,j} = 0. \quad \text{(C12f)}$$

The full conditions for Eq. (C10) are even more complicated. All we need to mention in this appendix is that one necessary condition is Eq. (C12b).

APPENDIX D: DOUGLAS-GUNN ADI METHOD

In this appendix we introduce the three-dimensional Douglas-Gunn ADI method [10,22,28,29] with operator splitting [22] and we investigate conditions for its material conservation. This method consists of the following five steps:

$$q^*_{\mathbf{i}} = \exp\left(-\frac{\Delta s}{2}w_{\mathbf{i}}\right)q^n_{\mathbf{i}}, \quad \text{(D1a)}$$
$$\left(1-a^2N\frac{\Delta s}{12}\delta_1^2\right)q^A_{\mathbf{i}} = \left(1+a^2N\frac{\Delta s}{12}\delta_1^2+a^2N\frac{\Delta s}{6}\delta_2^2 + a^2N\frac{\Delta s}{6}\delta_3^2\right)q^*_{\mathbf{i}}, \quad \text{(D1b)}$$
$$\left(1-a^2N\frac{\Delta s}{12}\delta_2^2\right)q^B_{\mathbf{i}} = q^A_{\mathbf{i}} - a^2N\frac{\Delta s}{12}\delta_2^2 q^*_{\mathbf{i}}, \quad \text{(D1c)}$$
$$\left(1-a^2N\frac{\Delta s}{12}\delta_3^2\right)q^{**}_{\mathbf{i}} = q^B_{\mathbf{i}} - a^2N\frac{\Delta s}{12}\delta_3^2 q^*_{\mathbf{i}}, \quad \text{(D1d)}$$
$$q^{n+1}_{\mathbf{i}} = \exp\left(-\frac{\Delta s}{2}w_{\mathbf{i}}\right)q^{**}_{\mathbf{i}}. \quad \text{(D1e)}$$

The bra-ket representation of Eqs. (D1) is

$$(\mathcal{I}-\mathcal{O}_1)|q^A\rangle = (\mathcal{I}+\mathcal{O}_1+2\mathcal{O}_2+2\mathcal{O}_3)\mathcal{X}|q^n\rangle, \quad \text{(D2a)}$$
$$(\mathcal{I}-\mathcal{O}_2)|q^B\rangle = |q^A\rangle - \mathcal{O}_2\mathcal{X}|q^n\rangle, \quad \text{(D2b)}$$
$$(\mathcal{I}-\mathcal{O}_3)\mathcal{X}^{-1}|q^{n+1}\rangle = |q^B\rangle - \mathcal{O}_3\mathcal{X}|q^n\rangle. \quad \text{(D2c)}$$

From these equations, the evolution operator is

$$\mathcal{U} = \mathcal{X}(\mathcal{I}-\mathcal{O}_3)^{-1}\{(\mathcal{I}-\mathcal{O}_2)^{-1}[(\mathcal{I}-\mathcal{O}_1)^{-1}(\mathcal{I}+\mathcal{O}_1+2\mathcal{O}_2+2\mathcal{O}_3)-\mathcal{O}_2]-\mathcal{O}_3\}\mathcal{X}. \tag{D3}$$

In order to verify whether the FVM conserves material, we are required to check if the following matrix is Hermitian when the $\mathcal{O}_d$'s for the FVM are adopted:

$$\mathcal{V}\mathcal{X}(\mathcal{I}-\mathcal{O}_3)^{-1}\{(\mathcal{I}-\mathcal{O}_2)^{-1}[(\mathcal{I}-\mathcal{O}_1)^{-1}(\mathcal{I}+\mathcal{O}_1+2\mathcal{O}_2+2\mathcal{O}_3)-\mathcal{O}_2]-\mathcal{O}_3\}\mathcal{X}. \tag{D4}$$

Using the theorem in Appendix B, the two $\mathcal{X}$ matrices in Eq. (D4) are removable and we only need to check the Hermiticity of the matrix

$$\mathcal{V}(\mathcal{I}-\mathcal{O}_3)^{-1}\{(\mathcal{I}-\mathcal{O}_2)^{-1}[(\mathcal{I}-\mathcal{O}_1)^{-1}(\mathcal{I}+\mathcal{O}_1+2\mathcal{O}_2+2\mathcal{O}_3)-\mathcal{O}_2]-\mathcal{O}_3\}\,. \tag{D5}$$

This equation becomes

$$\begin{aligned}
&\mathcal{V}(\mathcal{I}-\mathcal{O}_3)^{-1}\{(\mathcal{I}-\mathcal{O}_2)^{-1}[(\mathcal{I}-\mathcal{O}_1)^{-1}(\mathcal{I}+\mathcal{O}_1+2\mathcal{O}_2+2\mathcal{O}_3)-\mathcal{O}_2]-\mathcal{O}_3\}\\
&\quad=\mathcal{V}(\mathcal{I}-\mathcal{O}_3)^{-1}\{(\mathcal{I}-\mathcal{O}_2)^{-1}[(\mathcal{I}-\mathcal{O}_1)^{-1}(\mathcal{I}+\mathcal{O}_1+2\mathcal{O}_2+2\mathcal{O}_3)-\mathcal{O}_2]+\mathcal{I}-\mathcal{O}_3-\mathcal{I}\}\\
&\quad=\mathcal{V}(\mathcal{I}-\mathcal{O}_3)^{-1}(\mathcal{I}-\mathcal{O}_2)^{-1}(\mathcal{I}-\mathcal{O}_1)^{-1}(\mathcal{I}+\mathcal{O}_1+2\mathcal{O}_2+2\mathcal{O}_3)-\mathcal{V}(\mathcal{I}-\mathcal{O}_3)^{-1}(\mathcal{I}-\mathcal{O}_2)^{-1}\mathcal{O}_2+\mathcal{V}-\mathcal{V}(\mathcal{I}-\mathcal{O}_3)^{-1}.
\end{aligned} \tag{D6}$$

From Eq. (C5b), $\mathcal{V}(\mathcal{I}-\mathcal{O}_3)^{-1}$ is Hermitian and the last two terms can be removed in checking the Hermicity of the matrix. The remaining expression is

$$\mathcal{V}[(\mathcal{I}-\mathcal{O}_3)^{-1}(\mathcal{I}-\mathcal{O}_2)^{-1}(\mathcal{I}-\mathcal{O}_1)^{-1}(\mathcal{I}+\mathcal{O}_1+2\mathcal{O}_2+2\mathcal{O}_3)-(\mathcal{I}-\mathcal{O}_3)^{-1}(\mathcal{I}-\mathcal{O}_2)^{-1}\mathcal{O}_2]. \tag{D7}$$

Using Eqs. (C5), the conjugate transpose of Eq. (D7) turns out to be equivalent to

$$\begin{aligned}
&(\mathcal{I}+\mathcal{O}_1+2\mathcal{O}_2+2\mathcal{O}_3)^\dagger[(\mathcal{I}-\mathcal{O}_1)^{-1}]^\dagger[(\mathcal{I}-\mathcal{O}_2)^{-1}]^\dagger[(\mathcal{I}-\mathcal{O}_3)^{-1}]^\dagger\mathcal{V}-\mathcal{O}_2{}^\dagger[(\mathcal{I}-\mathcal{O}_2)^{-1}]^\dagger[(\mathcal{I}-\mathcal{O}_3)^{-1}]^\dagger\mathcal{V}\\
&\quad=\mathcal{V}[(\mathcal{I}+\mathcal{O}_1+2\mathcal{O}_2+2\mathcal{O}_3)(\mathcal{I}-\mathcal{O}_1)^{-1}(\mathcal{I}-\mathcal{O}_2)^{-1}(\mathcal{I}-\mathcal{O}_3)^{-1}-\mathcal{O}_2(\mathcal{I}-\mathcal{O}_2)^{-1}(\mathcal{I}-\mathcal{O}_3)^{-1}].
\end{aligned} \tag{D8}$$

Our final task is to compare the two equations (D7) and (D8). Multiplying $(\mathcal{I}-\mathcal{O}_1)(\mathcal{I}-\mathcal{O}_2)(\mathcal{I}-\mathcal{O}_3)\mathcal{V}^{-1}$ from the left and $(\mathcal{I}-\mathcal{O}_3)(\mathcal{I}-\mathcal{O}_2)(\mathcal{I}-\mathcal{O}_1)$ from the right of both expressions, one obtains the equation

$$\begin{aligned}
&[(\mathcal{I}+\mathcal{O}_1+2\mathcal{O}_2+2\mathcal{O}_3)-(\mathcal{I}-\mathcal{O}_1)\mathcal{O}_2]\\
&\quad\times(\mathcal{I}-\mathcal{O}_3)(\mathcal{I}-\mathcal{O}_2)(\mathcal{I}-\mathcal{O}_1)\\
&=(\mathcal{I}-\mathcal{O}_1)(\mathcal{I}-\mathcal{O}_2)(\mathcal{I}-\mathcal{O}_3)\\
&\quad\times[(\mathcal{I}+\mathcal{O}_1+2\mathcal{O}_2+2\mathcal{O}_3)-\mathcal{O}_2(\mathcal{I}-\mathcal{O}_1)].
\end{aligned} \tag{D9}$$

The material conservation is guaranteed if this equation is true. For the two-dimensional case, we set $\mathcal{O}_3=0$ and Eq. (D9) reduces to $\mathcal{O}_1\mathcal{O}_2^2=\mathcal{O}_2^2\mathcal{O}_1$. It is the same equation obtained in the previous appendix except that the roles of indices 1 and 2 are reversed.

For the two-dimensional systems, all the remaining stories of the basic ADI method can be shared. This means that material conservation fails in the two-dimensional cylindrical and spherical coordinate system while the Cartesian coordinate system has the ability to conserve the amount of material, when the FVM with operator splitting Douglas-Gunn ADI method is adopted.

Because material conservation fails in most coordinate systems for the two-dimensional Douglas-Gunn ADI method, we only need to check the material conservation of the three-dimensional case for the Cartesian coordinate system. In this case, the $\mathcal{O}_d$'s commute, Eq. (D9) is satisfied, and the operator splitting Douglas-Gunn ADI method in the Cartesian coordinate system conserves material. In short, most of our conclusions in this paper can be directly extended to the three-dimensional numerical SCFT schemes.

[1] F. S. Bates and G. H. Fredrickson, Phys. Today **52**(2), 32 (1999).

[2] M. W. Matsen, in *Soft Matter*, edited by G. Gompper and M. Schick (Wiley-VCH, Weinheim, 2006), Vol. 1.

[3] G. H. Fredrickson, *The Equilibrium Theory of Inhomogeneous Polymer* (Oxford University Press, New York, 2006).

[4] K. Ø. Rasmussen and G. Kalosakas, J. Polym. Sci. B **40**, 1777 (2002).

[5] H. D. Ceniceros and G. H. Fredrickson, Multiscale Model. Simul. **2**, 452 (2004).

[6] E. W. Cochran, C. J. Garcia-Cervera, and G. H. Fredrickson, Macromolecules **39**, 2449 (2006).

[7] A. Ranjan, J. Qin, and D. C. Morse, Macromolecules **41**, 942 (2008).

[8] P. Stasiak and M. W. Matsen, Eur. Phys. J. E **34**, 110 (2011).

[9] D. Lee, M.-H. Kim, D. Bae, G. Jeon, M. Kim, J. Kwak, S. J. Park, J. U. Kim, and J. K. Kim, Macromolecules **47**, 3997 (2014).

[10] Y.-B. Yang, Y. M. Jeon, J. U. Kim, and J. Cho, Eur. Phys. J. E **35**, 86 (2012).

[11] F. Drolet and G. H. Fredrickson, Phys. Rev. Lett. **83**, 4317 (1999).

[12] F. Drolet and G. H. Fredrickson, Macromolecules **34**, 5317 (2001).

[13] P. Tang, F. Qiu, H. Zhang, and Y. Yang, Phys. Rev. E **72**, 016710 (2005).
[14] J. F. Li, J. Fan, H. D. Zhang, F. Qiu, P. Tang, and Y. L. Yang, Eur. Phys. J. E **20**, 449 (2006).
[15] J. U. Kim and M. W. Matsen, Macromolecules **41**, 246 (2008).
[16] G. H. Fredrickson, V. Ganesan, and F. Drolet, Macromolecules **35**, 16 (2002).
[17] J. U. Kim and M. W. Matsen, Phys. Rev. Lett. **102**, 078303 (2009).
[18] J. U. Kim and M. W. Matsen, Soft Matter **5**, 2889 (2009).
[19] B. Vorselaars, J. U. Kim, T. L. Chantawansri, G. H. Fredrickson, and M. W. Matsen, Soft Matter **7**, 5128 (2011).
[20] J. Li, H. Zhang, and F. Qiu, Eur. Phys. J. E **37**, 18 (2014).
[21] W. H. Press, B. P. Flannery, S. A. Teukolsky, and W. T. Vetterling, *Numerical Recipes: The Art of Scientific Computing* (Cambridge University Press, Cambridge, 2007).
[22] Y.-B. Yang, S. J. Park, P. Kim, and J. U. Kim, Soft Matter **9**, 5624 (2013).
[23] R. J. LeVeque, *Finite Volume Methods for Hyperbolic Problems* (Cambridge University Press, Cambridge, 2002).
[24] A. Mignone, J. Comput. Phys. **270**, 784 (2014).
[25] G. Tzeremes, K. Ø. Rasmussen, T. Lookman, and A. Saxena, Phys. Rev. E **65**, 041806 (2002).
[26] J. Douglas, Jr., Numer. Math. **4**, 41 (1962).
[27] H. Zeng and J. Zhu, *Proceedings of the International Conference on Parallel Processing Workshops* (IEEE, 2002), p. 320.
[28] M. Sun, P. Wang, F. Qiu, P. Tang, H. Zhang, and Y. Yang, Phys. Rev. E **77**, 016701 (2008).
[29] D.-W. Sun, Z.-Y. Sun, H.-F. Li, and L.-J. An, Polymer **50**, 4270 (2009).
[30] Y.-B. Yang, Y. J. Choi, S. O. Kim, and J. U. Kim, Soft Matter **11**, 4496 (2015).
[31] J. U. Kim and M. W. Matsen, Macromolecules **41**, 4435 (2008).
[32] C.-W. Shu, Int. J. Comput. Fluid Dyn. **17**, 107 (2003).
[33] Y. Liu, C.-W. Shu, and M. Zhang, SIAM J. Sci. Comput. **33**, 939 (2011).
[34] P. Colella and P. R. Woodward, J. Comput. Phys. **54**, 174 (1984).
[35] B. H. Kim, H. M. Lee, J.-H. Lee, S.-W. Son, S.-J. Jeong, S. Lee, D. I. Lee, S. U. Kwak, H. Jeong, H. Shin, J.-B. Yoon, O. D. Lavrentovich, and S. O. Kim, Adv. Funct. Mater. **19**, 2584 (2009).
[36] P. Stasiak, J. D. McGraw, K. Dalnoki-Veress, and M. W. Matsen, Macromolecules **45**, 9531 (2012).
[37] A. Knoll, A. Horvat, K. S. Lyakhova, G. Krausch, G. J. A. Sevink, A. V. Zvelindovsky, and R. Magerle, Phys. Rev. Lett. **89**, 035501 (2002).
[38] T. Wang and C. C. Chen, IEEE Trans. Very Large Scale Integr. Syst. **11**, 691 (2003).